Numerical Studies of Harmonic Cavity Effects in NSLS-II and MAX-IV

G. Bassi, A. Blednykh, J. Tagger
Brookhaven National Laboratory, Upton, NY

BROOKHAVEN NATIONAL LABORATORY

NATIONAL SYNCHROTRON LIGHT SOURCE II

Self-consistent Parallel Tracking Code SPACE*

(Self-consistent Parallel Algorithm for Collective Effects)

General Features and Capabilities

- Efficient study of short and long-range wakefield effects in 6D phase-space.
- Study of slow head-tail effect + coupled-bunch instabilities.
- Passive higher harmonic cavity effects with arbitrary fillings.
- Microwave instability.
- Efficient density estimation methods from particles.
- Localized wakefield effects.
- A model of the transverse feedback system.

General Parallel Structure

- M bunches, each with N simulations particles, are distributed to M processors.
- Short-range (single bunch) wakefield interaction calculated in serial (locally).
- Long-range wakefield calculation done in parallel (globally) via master-to-slave processor communications by storing the "history" of bunch moments.
- For efficient study of microwave instability, the calculation is done in parallel by distributing N/M simulation particles to M processors.

Future Additions

Develop a model of:

- Ion effects.
- Low Level RF System.

* G. Bassi, A. Blednykh and V. Smaluk, "Self-consistent Simulations and Analysis of the Coupled Bunch Instability for Arbitrary Multi-bunch Configurations", Phys. Rev. Acc. Beams **19**, 024401, (2016).

NSLS-II Storage Ring Parameters

(with 3 Damping Wigglers)

Parameter	Value
Beam energy	E = 3GeV
Average Current	I = 500mA
Number of bunches	M =1000
Harmonic number	h = 1320
Circumference	C= 792m
Bunch length w/o HC	σ_τ= 14.5ps
Energy Spread	σ_δ =8.7x10^{-4}
Energy loss per turn	U_s=2MeV
Momentum compaction	η=3.67x10^{-4}
Long. radiation damping	τ_{rad}=11.9ms

Super Conducting Cavity System:

2 MAIN cavities + **3rd HARMONIC** cavity

Per cavity parameter	Value
RF frequency (main)	f_{rf} = 499.68MHz
RF frequency (harmonic)	3f_{rf} = 1499.04MHz
RF voltage	V = 1.23MV
Beta coupling	β = 9615
Shunt impedance (main)	R_L = 33375 MΩ
Quality factor (main)	Q_L =78000
Shunt impedance (harmonic)	R_H = 22880 MΩ
Quality factor (harmonic)	Q_H = 2.6x10^8

Theoretical Bunch Lengthening from Active 3rd HC

(same for passive HC with uniform fillings)

bunch lengthening u for an equilibrium distribution ρ_e in quartic potential

$$u := \frac{\sigma_{\tau L}}{\sigma_{\tau m}} = \left(\frac{\Gamma(3/4)}{\Gamma(1/4)}\right)^{1/2}\left(\frac{24\cos\phi_{s0}}{(m^2-1)\omega_{rf}^2\cos\phi_s}\right)^{1/4}\frac{1}{\sqrt{\sigma_{\tau m}}} \quad (18)$$

where Γ is the Gamma function, $\sigma_{\tau_m} = \frac{\eta}{\omega_{s0}}\sigma_\delta$ is the equilibrium bunch length with only the main cavity, and σ_{τ_L} is the equilibrium bunch length with the Landau cavity. The For the NSLS-II SR with $\sigma_{\tau m}$ = 14.5 ps ⇨ $u = 3.7$

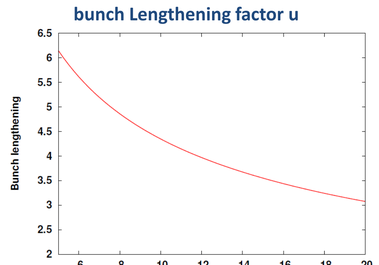

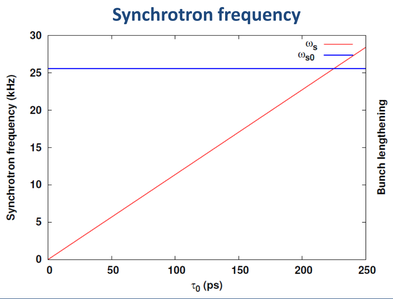

Bunch Lengthening in NSLS-II: Measurements

(W.Cheng, B. Bacha, Mar 4, 2016)

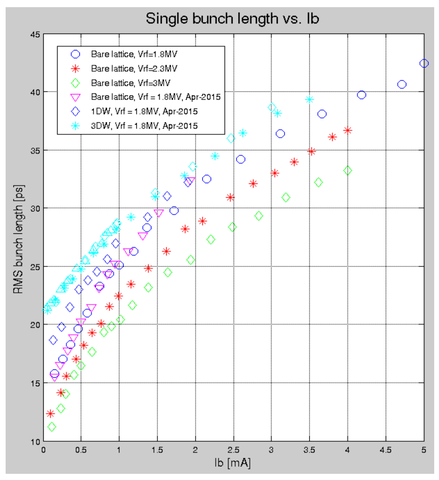

Single bunch length increase ~ 10ps/1mA

Simulations of Active HC + Bunch Lengthening

(Uniform Fillings)

SPACE simulations with the current longitudinal impedance budget

3rd HC OFF

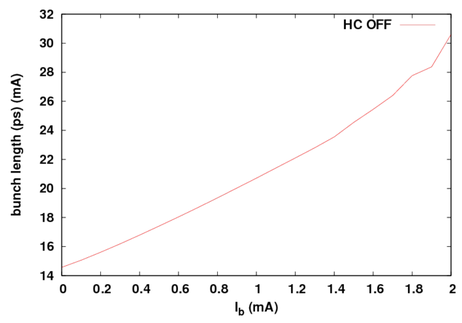

3rd HC ON

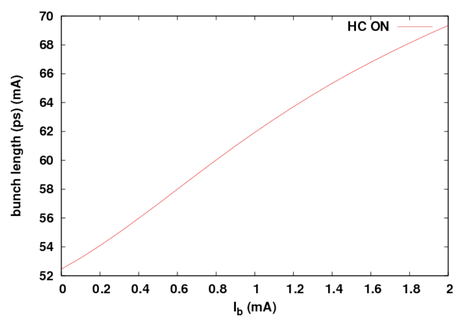

Bunch lengthening from 3rd HC weakly affected by longitudinal Impedance

Passive Harmonic Cavity in MAX-IV with a Gap in the Fillings

(case study, IPAC13 paper MOPB03)

Storage Ring Parameters

(with gap of 44 bunches in the fillings)

Parameter	Value
Beam energy	E = 3GeV
Average Current	I = 500mA
Number of bunches	M = 132
Harmonic number	h = 176
Circumference	C= 528m
Bunch length w/o HC	σ_τ= 40ps
Energy Spread	σ_p=7.7x10^{-4}
Energy loss per turn	U_s=364keV
Momentum compaction	η=3.07x10^{-4}
Long. radiation damping	τ_{rad}=25ms

Normal Conducting Cavity System:

4 MAIN and **1 LANDAU** (3rd harmonic) cavity

Per cavity parameter	Value
RF frequency (main)	f_{rf} = 99.93MHz
RF frequency (Landau)	mf_{rf} = 299.79MHz
RF voltage	V=0.255MV
Beta coupling	β=1.9
Shunt impedance (main)	R_L =1.759 MΩ
Shunt impedance (Landau)	Q_L =20946
Quality factor (main)	R_H =1.759 MΩ
Quality factor (Landau)	Q_H =20946

Uniform Fillings

(**nominal** configuration):

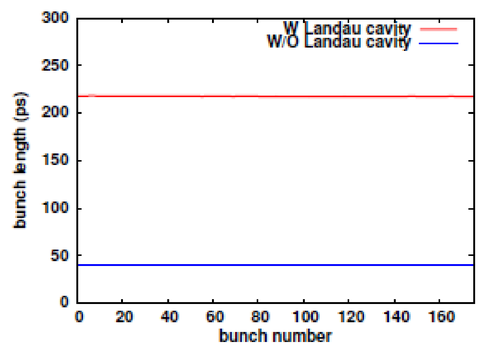

Gap (44) in the Fillings in MAX-IV

Self-consistent simulations with SPACE

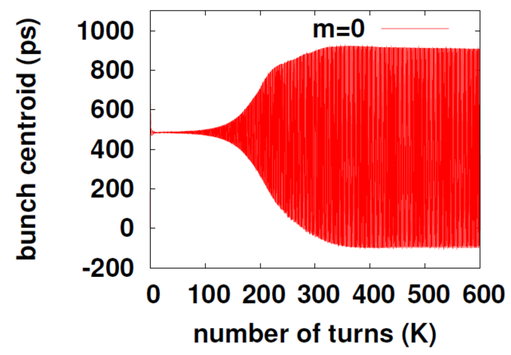

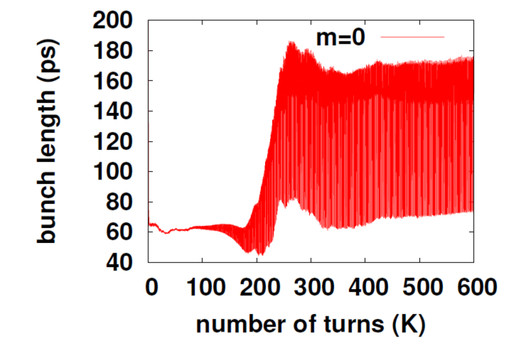

Instability with saturation

Gap (44) in the Fillings in MAX-IV

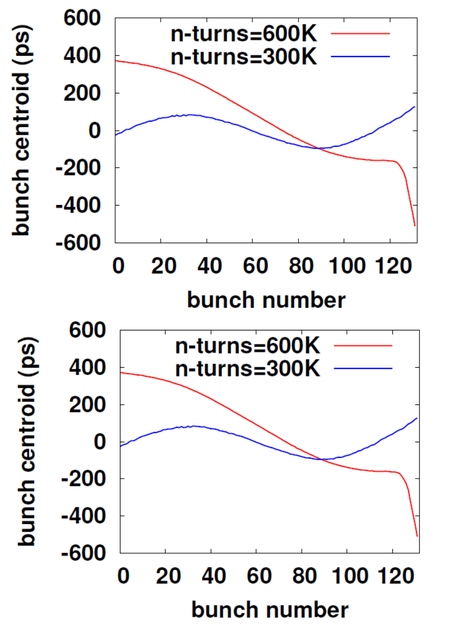

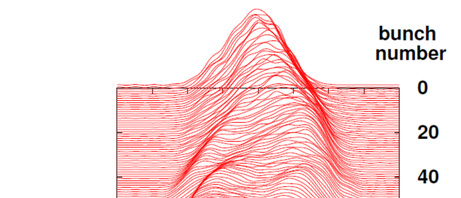

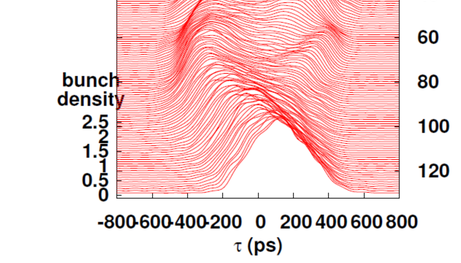

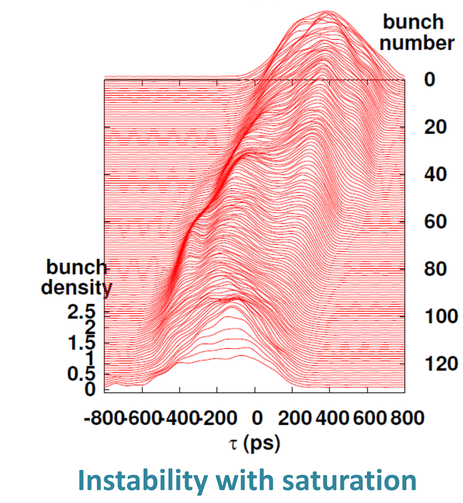

Instability with saturation

Stabilizing Effect by Decreasing the Radiation Damping Time

τ_{rad}= 25ms ⇨ τ_{rad}= 1.57ms

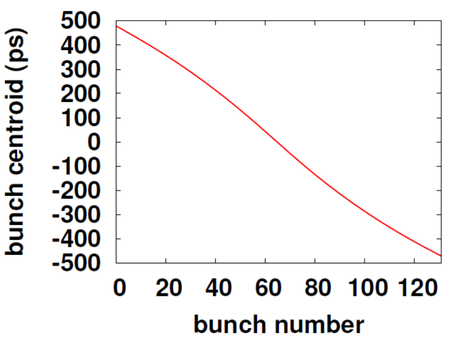

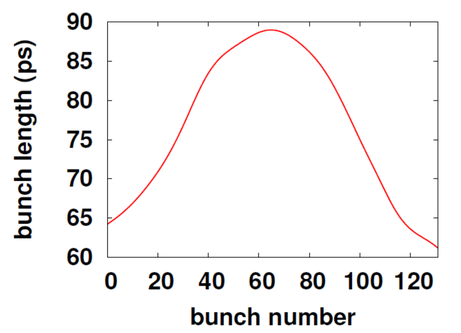

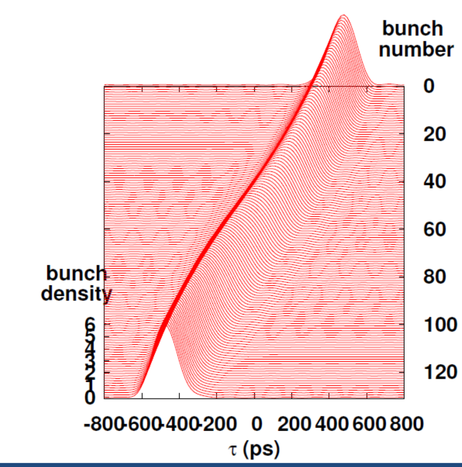

BEAM-INDUCED HEATING OF THE KICKER CERAMICS CHAMBERS AT NSLS-II

BNL, NSLS-II, Upton, New York, 11973-5000, U.S.A.

A. Blednykh, B. Bacha, G. Bassi, G. Ganetis, C. Hetzel, H.-C. Hseuh, V. Smalyuk, T. Shaftan, G. Wang

NATIONAL SYNCHROTRON LIGHT SOURCE II

First experience with the beam-induced heating of the ceramics chambers in the NSLS-II storage ring has been discussed. Total five ceramics chambers are considered to be replaced due to overheating concern during of upcoming $I_{av} = 500mA$ operations. The air cooling fans has been installed as a temporarily solution to remove heat. Four ceramic chambers with 2 microns titanium (Ti) coating are installed in the injection straight section (Cell 30) and one the same chamber is installed at different straight section (Cell 22) in pinger location. The schematic layout of the injection straight section is shown in Fig. 1. The kicker ceramic chambers have a ceramic length of 755 mm and octagonal profile.

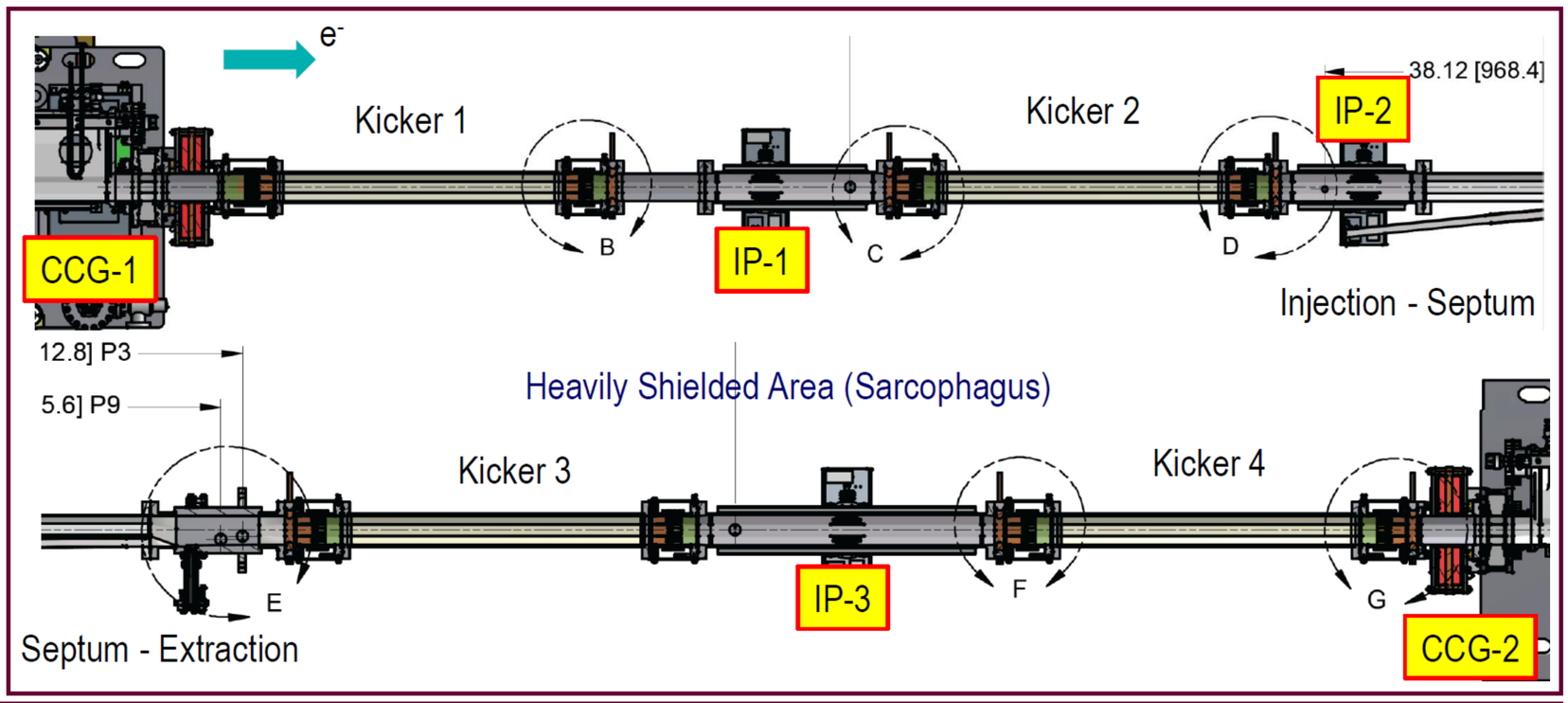

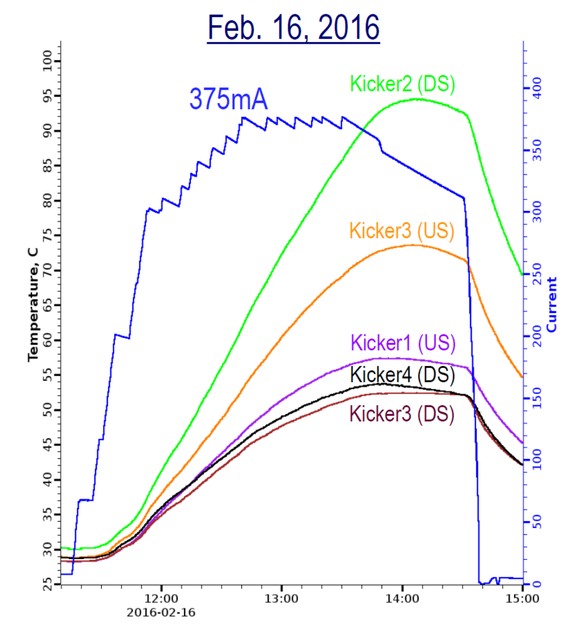

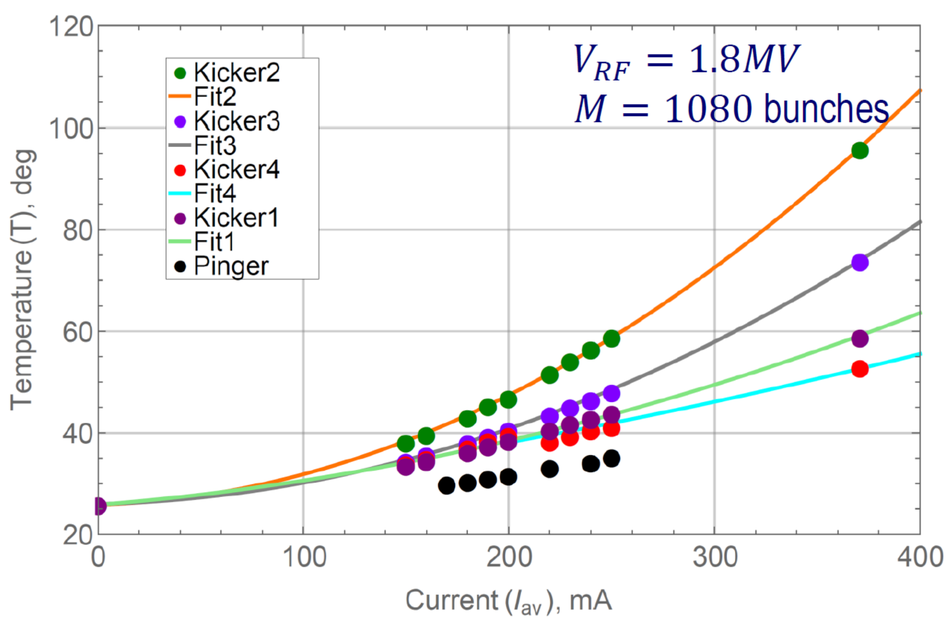

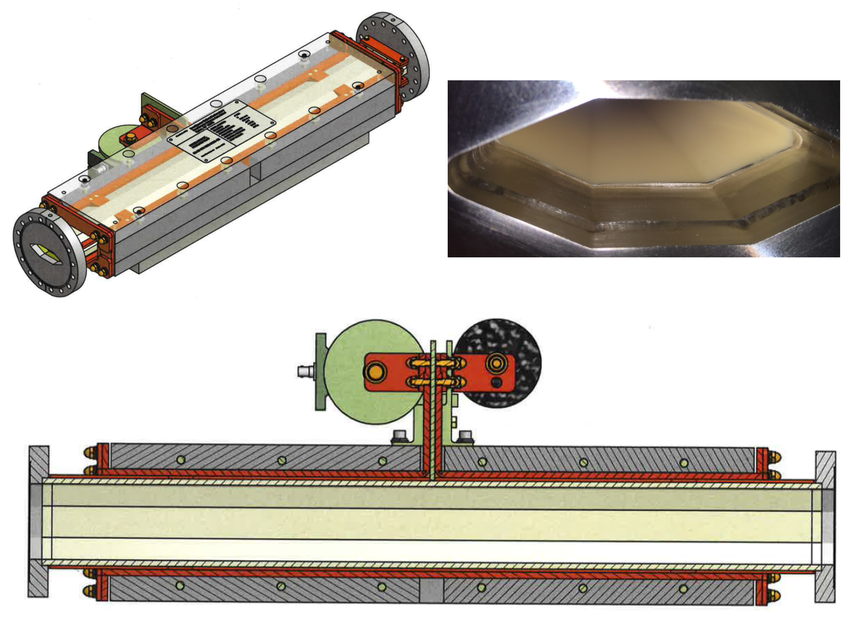

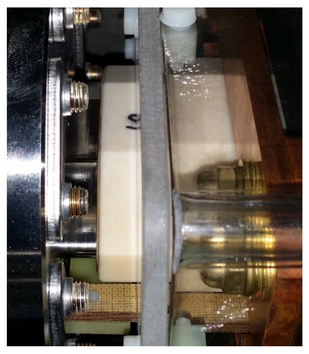

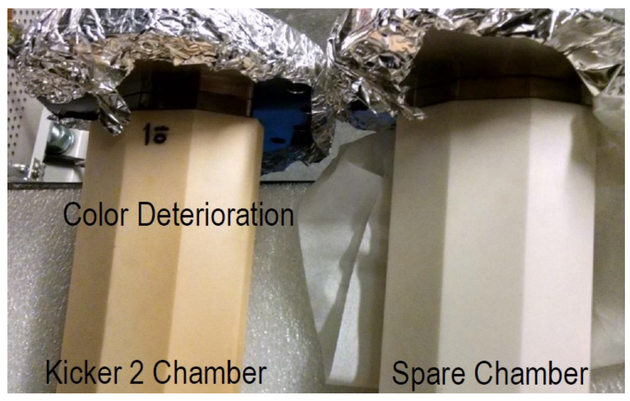

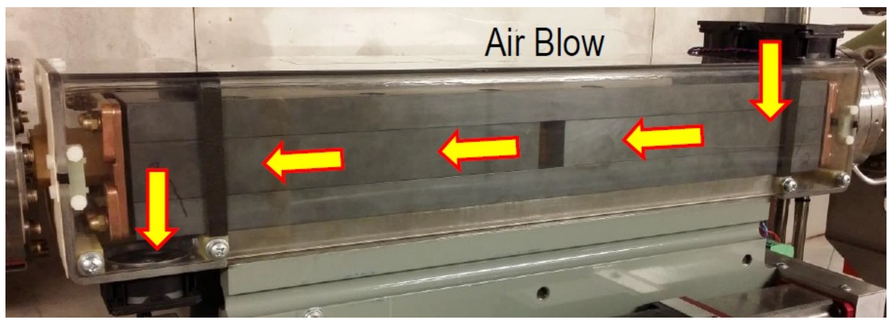

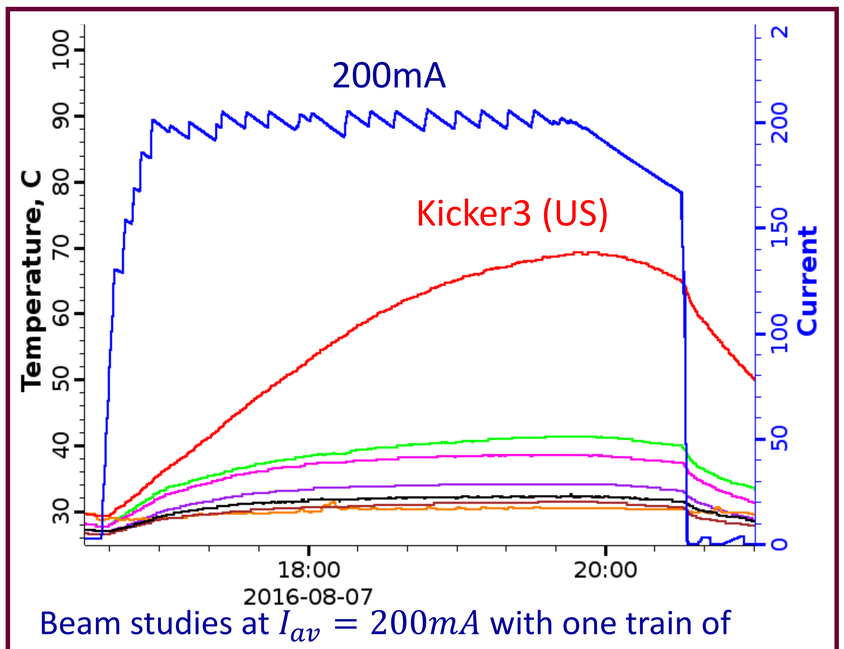

Beam studies at $I_{av} = 200mA$ with one train of $M = 270$ bunches

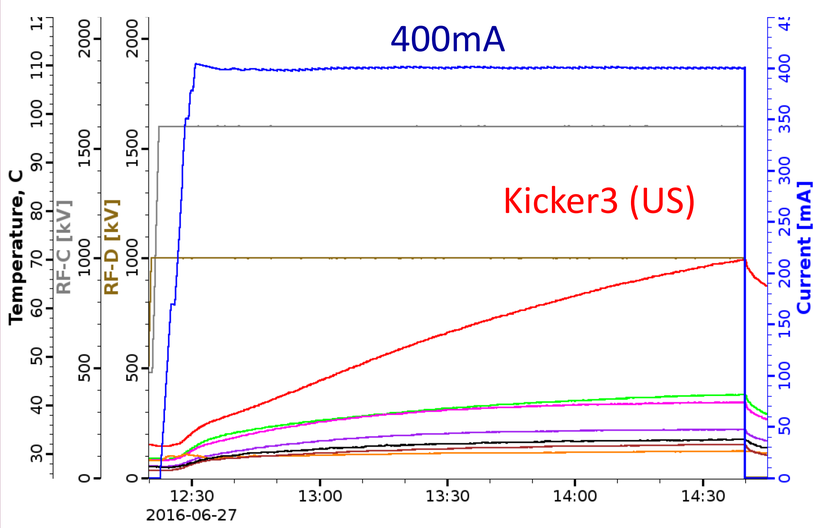

Beam studies at $I_{av} = 400mA$ with one train of $M = 1080$ bunches

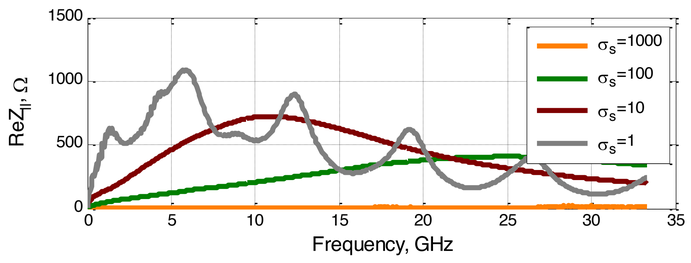

Real part of the longitudinal impedance simulated by the GdfidL code up to 32GHz for different electrical conductivities of the ceramics chamber.

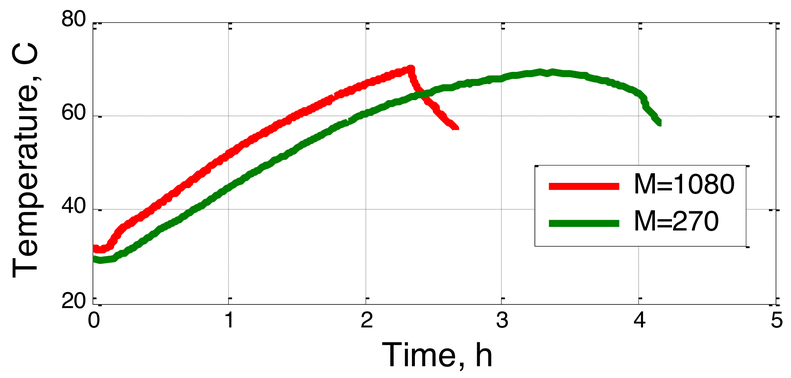

Temperature rise comparison as a function of time. Time is in hours. Number of bunches is M

HIGH BRIGHTNESS LATTICE UPGRADE

Eric B. Blum and Weiming Guo

BROOKHAVEN NATIONAL LABORATORY

Goals-

1. Reduce storage ring horizontal emittance by as much as 4x
2. Do this as inexpensively as possible

Possibilities-

Minimizing $\langle \mathcal{H} \rangle$

Theoretical limit: 1nm, versus 2nm
Theoretical minimal betax: 0.25m, versus 0.68m
Not effective, 10-15% reduction limited by the sextupole strength

Relaxing the achromat condition(long straights only): theoretical 0.7nm

50% reduction achievable while maintaining similar lattice functions
Damping wiggler sections must be dispersion-free
Users of the long straights will not benefit

Emittance reduction by changing damping partition numbers

Replacing dipoles to build a 4-bend achromat

Major upgrade
Challenging nonlinear optimization
But 4-5x emittance reduction possible

Changing Damping Partition

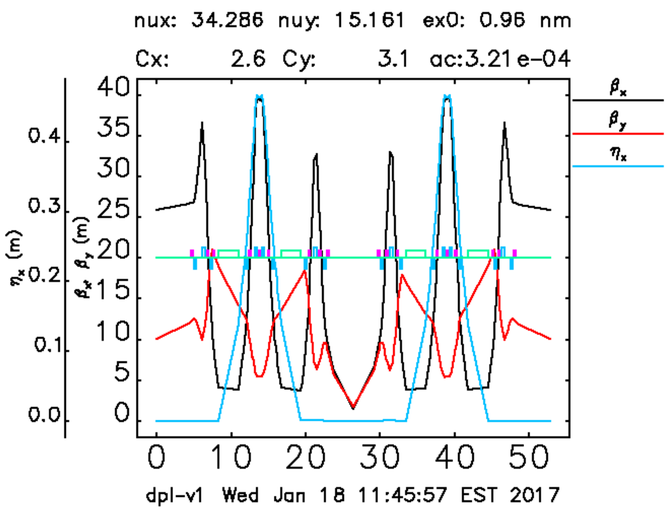

- Increase dipole current by about 5-10A.
- Peak orbit change is about -6mm
- Rematch the quadrupoles

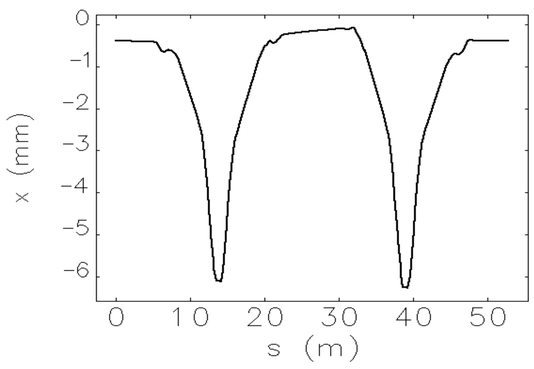

Emit	Sig d	Jx	JE
1 nm	0.06%	1.58	1.42
2 nm	0.05%	1.0	2.0

4-Bend Achromat

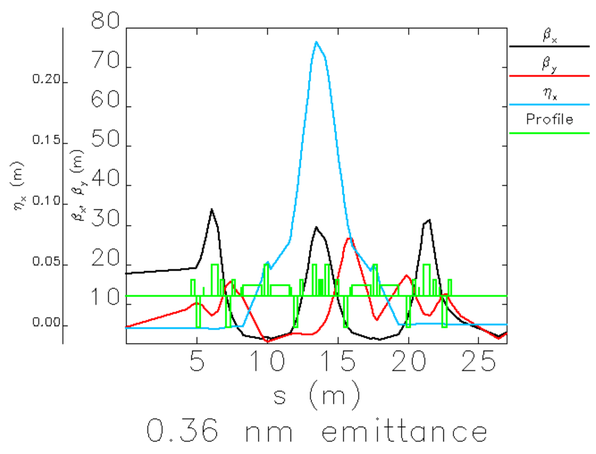

Lattice Properties

nux	44.08
dnux/dp	-142.69
nuy	30.66
dnuy/dp	-78.76
alphac2	2.06e-3
alphac	2.29e-4
Jx	1.87

Requires sextupoles K_2 3-4x stronger than NSLS-II

Advances in NSLS-II Beam Diagnostics

Weixing Cheng
NSLS-II, Brookhaven National Laboratory, Upton, NY 11973
 # chengwx@bnl.gov

BROOKHAVEN NATIONAL LABORATORY

NATIONAL SYNCHROTRON LIGHT SOURCE II

BPM

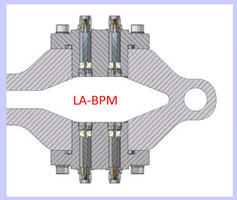

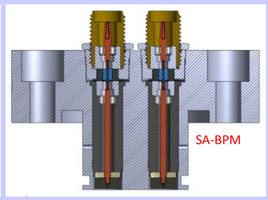

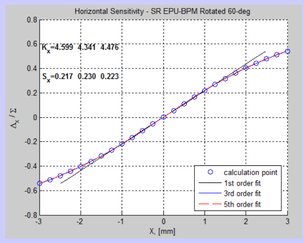

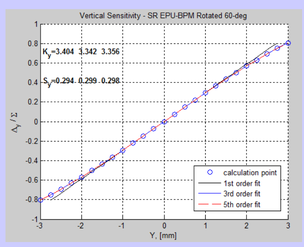

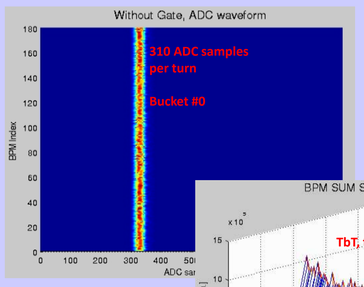

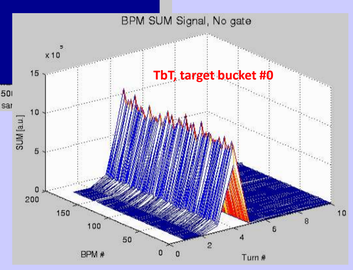

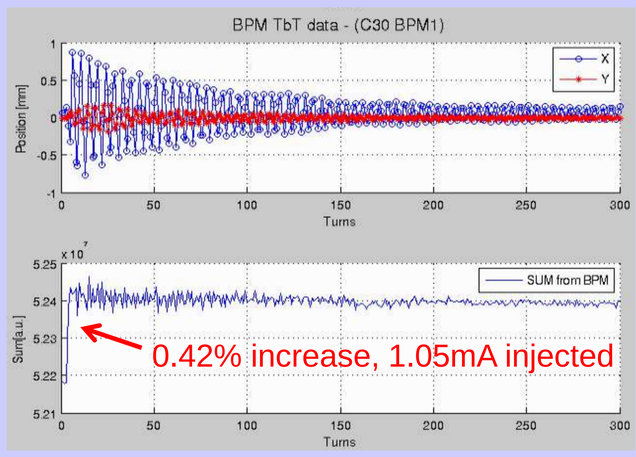

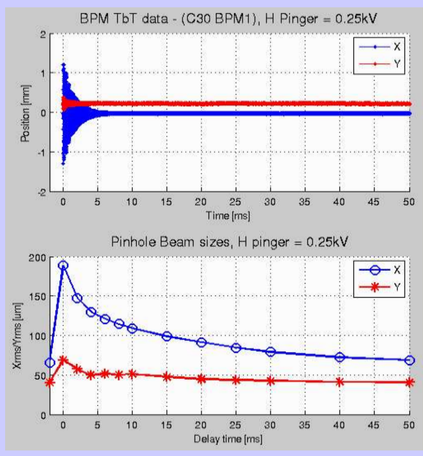

(Left) BPM turn by turn position transient during top-off operation.

(Right) Measured beam centroid (BPM TbT) and beam sizes (X-ray pinhole) after pulse kick. Pinhole images were saved with different delay to the pulse kick. Exposure time was at 2ms.

Synchrotron Light Monitor

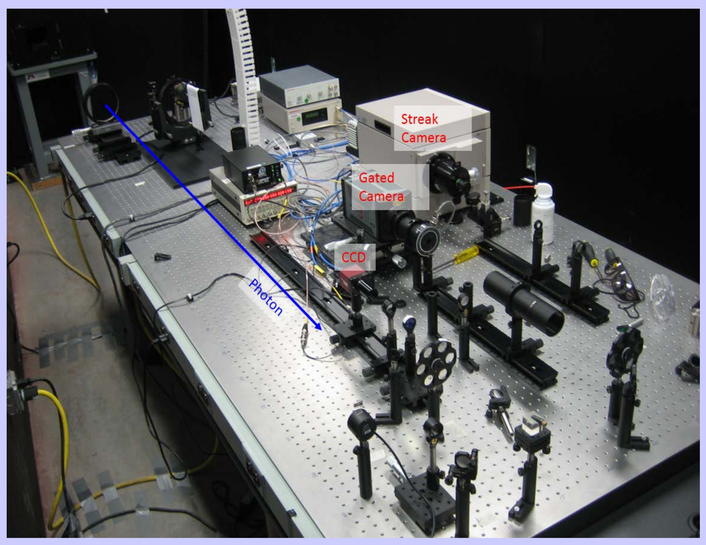

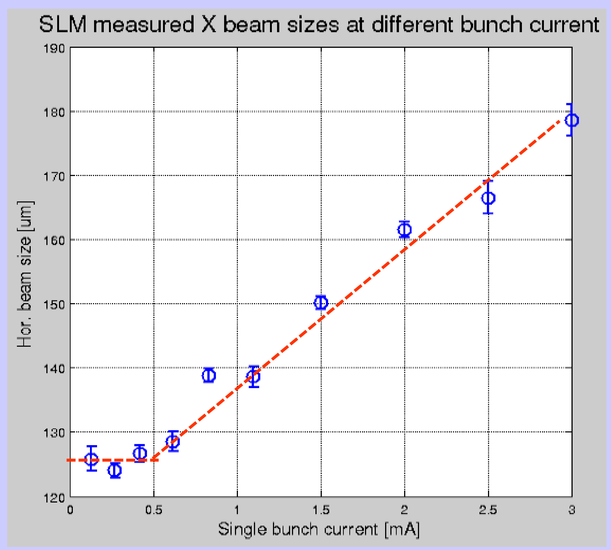

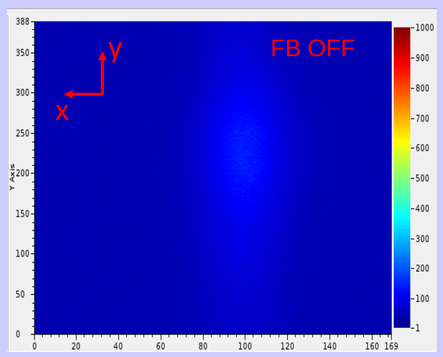

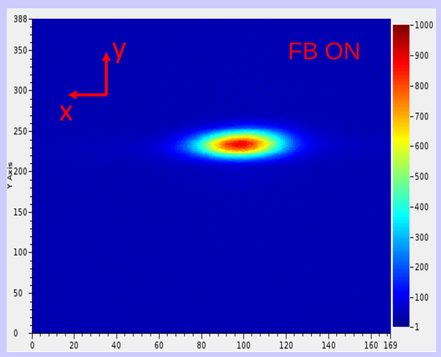

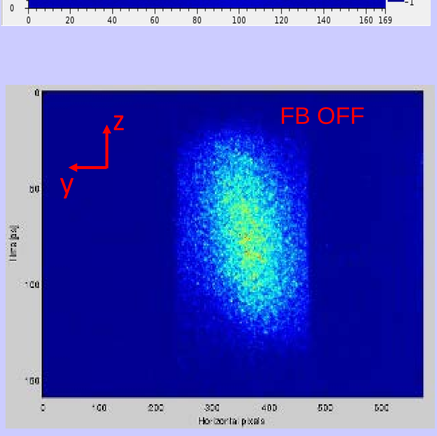

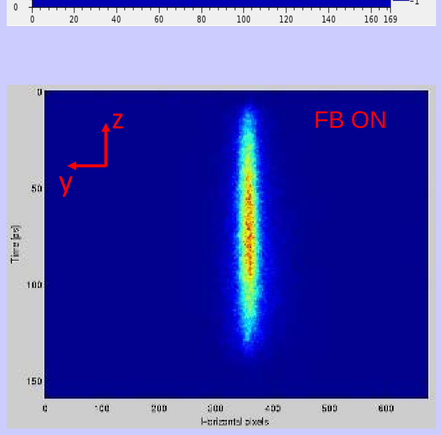

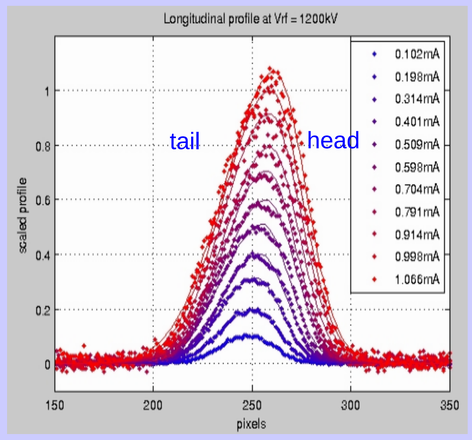

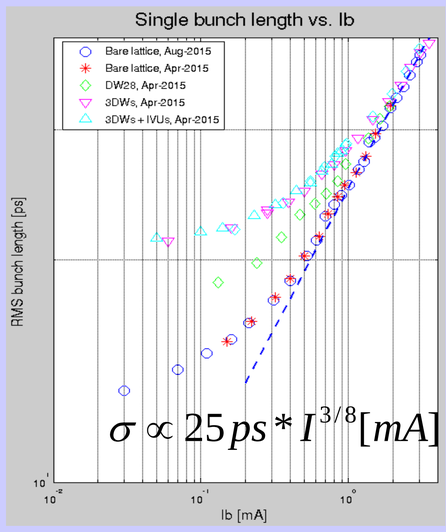

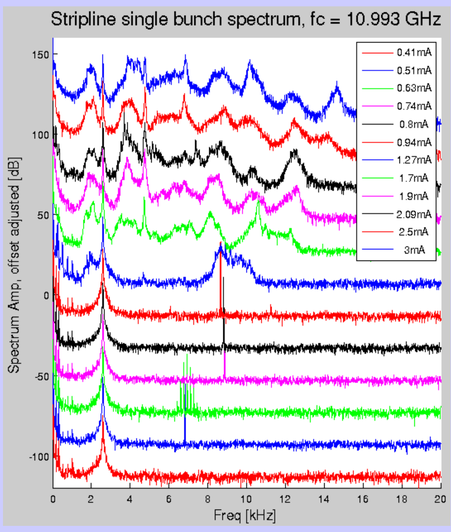

(top) SLM CCD camera images with single bunch current stored at TMCI threshold current of 0.8mA. x-y profile was measured on the CCD images. (bottom) y-z streak camera image at the same single bunch current.

Bunch by Bunch Feedback and Monitoring

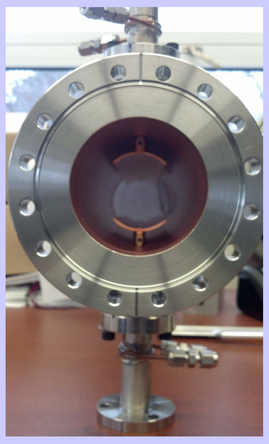

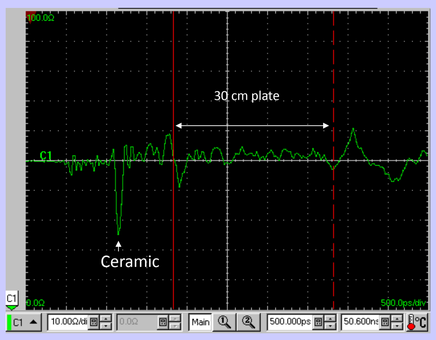

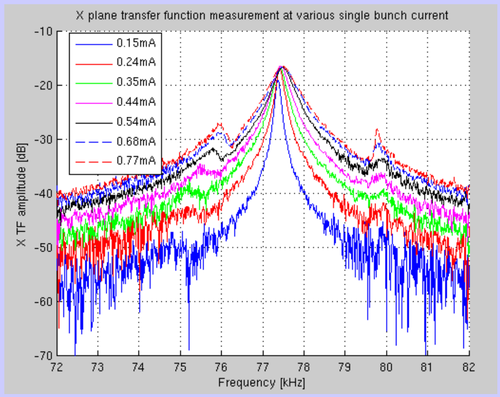

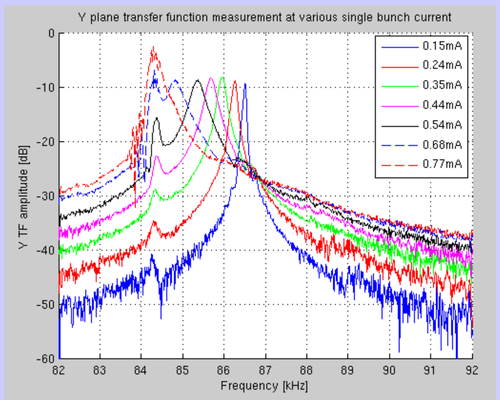

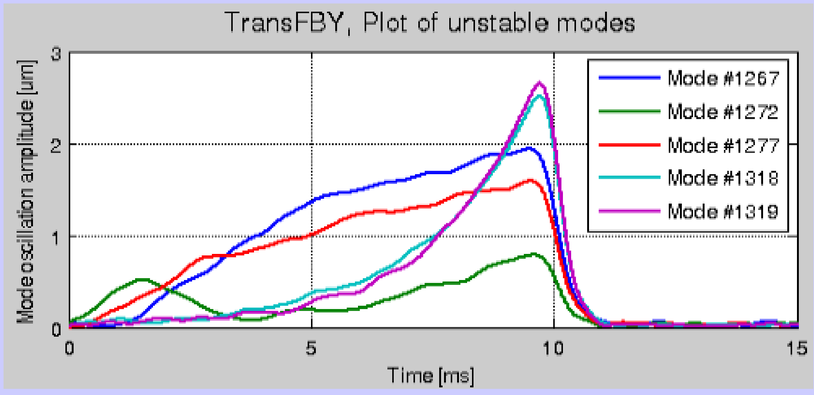

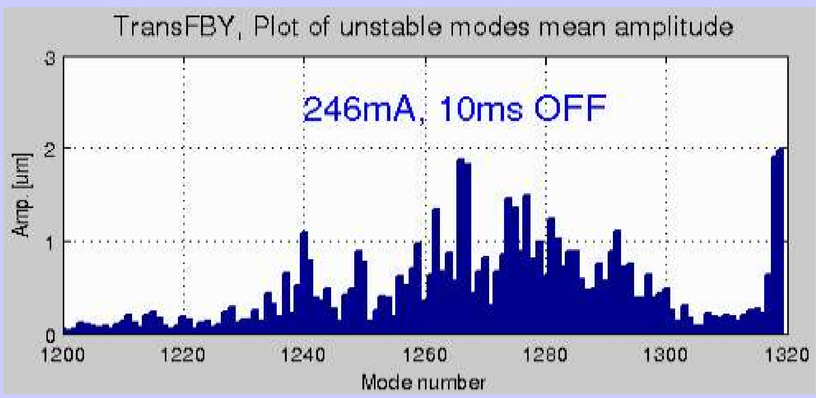

Lattice with 15 Insertion Devices

W. Guo, Y. Hidaka, X. Yang

BROOKHAVEN NATIONAL LABORATORY

NATIONAL SYNCHROTRON LIGHT SOURCE II

Totally 15 insertion devices have been installed and 12 are in daily operations. This poster shows the lattice adjustments to the changes. In particular, every insertion device is modeled as a kick-map, the linear lattice has been re-matched, the skew quadrupole components were corrected, and the nonlinear dynamics was re-examined.

List of IDs and their parameters

Beam Line	Project	Type	Location	Length [m]	Period [mm]	Mag Gap [mm]	Canting Angle [mrad]
CSX1/CSX2	NSLS-II	EPU49	23-ID	4 (2×2)	49	11.5	0.16
IXS	NSLS-II	IVU22	10-ID	6 (2×3) center	22	7.4	0
HXN	NSLS-II	IVU20	3-ID	3	20	5.2	0
CHX	NSLS-II	IVU20	11-ID	3	20	5.2	0
SRX/(XFN)	NSLS-II	IVU21	5-ID	1.5 downstream	21	6.4	2.0
XPD/PDF	NSLS-II	DW100	28-ID	6.8 (2×3.4)	100	15.0	
ESM*	NEXT	EPU105/ EPU57	21-ID	2.7(downstream) /1.4 (upstream) *no canting	105/49	16.0	2.0
SIX*	NEXT	EPU57	2-ID	7.0 (2×3.5)	57	16.0	0
ISR	NEXT	IVU23	4-ID	2.8	23	6.2	2.0
SMI	NEXT	IVU23	12-ID	2.8	23	6.2	2.0
ISS+XFP	NEXT	DW100	18-ID	6.8 (2×3.4)	100	15.0	
FXI	NEXT	DW100	8-ID	6.8 (2×3.4)	100	15.0	
LIX	ABBIX	IVU23	16-ID	2.8	23	5.7	0
FMX/AMX	ABBIX	IVU21	17-ID	1.5	21	6.4	2.0
NYX*	Partner	IVU18	19-ID	1.0 (upstream)	18	5.6	0

❖ IDs, canting magnets, and user BPMs were put into the lattice at their exact locations.

Re-matched Linear Lattice

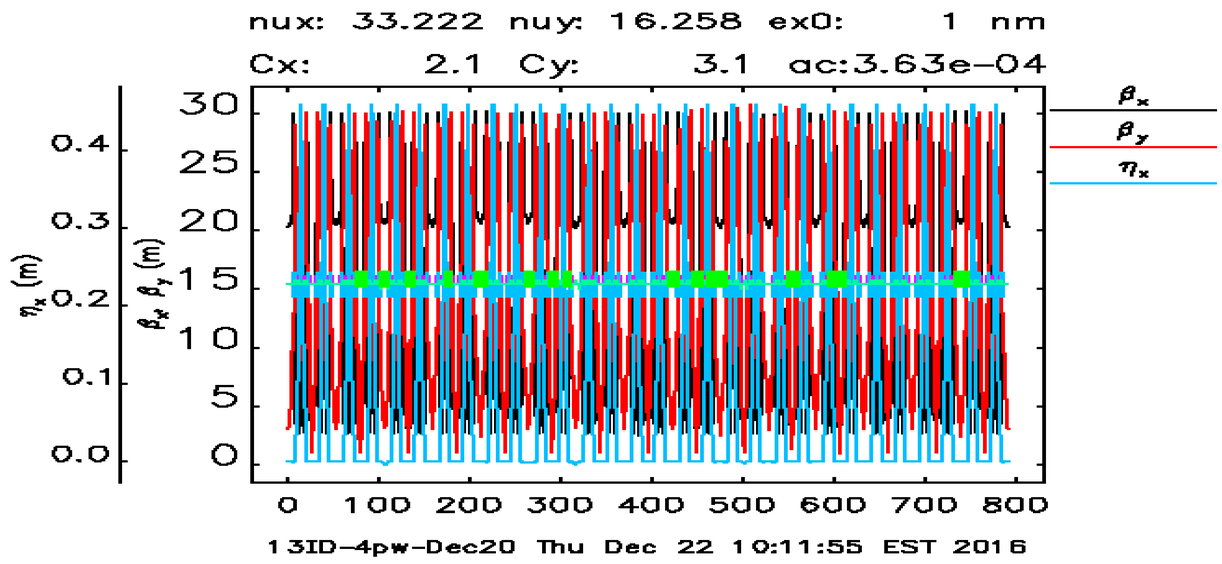

❖ Quadrupole families have the same settings except those in the ID sections
❖ Phase advance as well as beta functions were restored
❖ Skew quadrupoles were modeled using the ID measurement data; however, the actual correction was carried out online.
❖ Sextupole settings were kept the same as the bare lattice.

Frequency Map in (x,δ) space

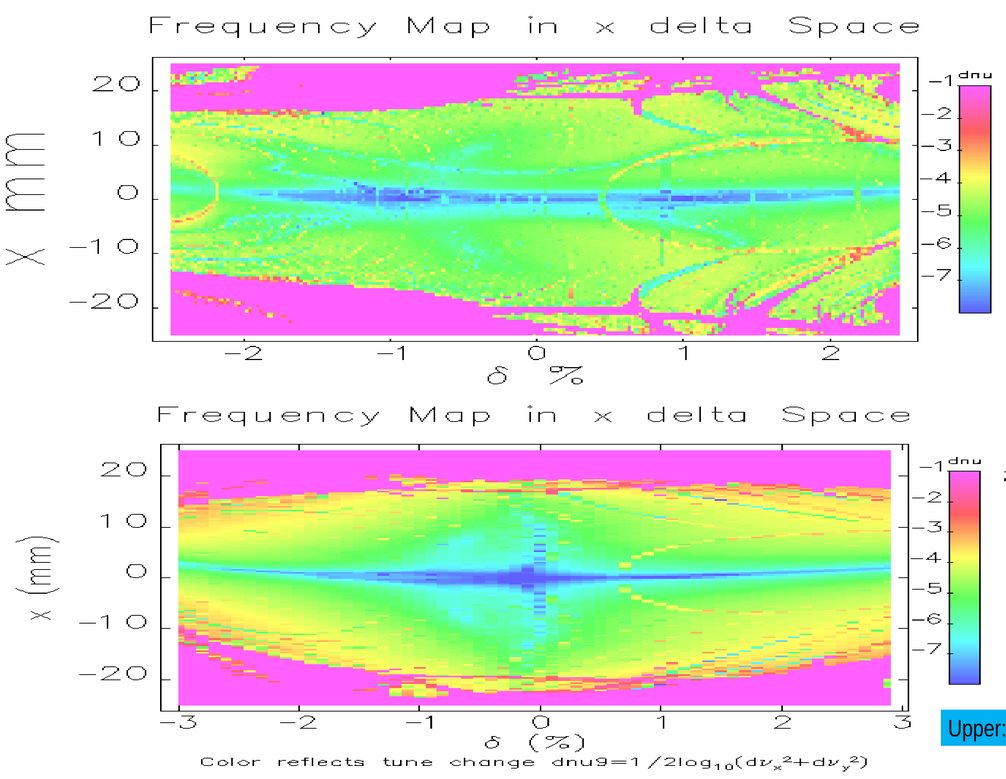

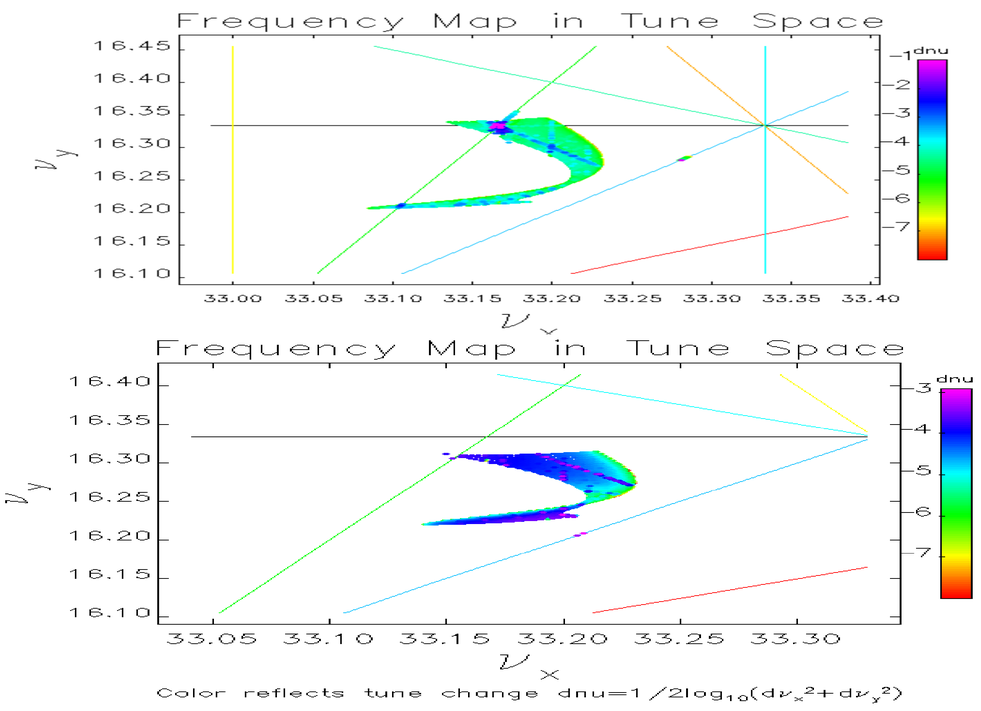

Upper: with 12 IDs, lower: bare lattice

Frequency Map in (x,y) space

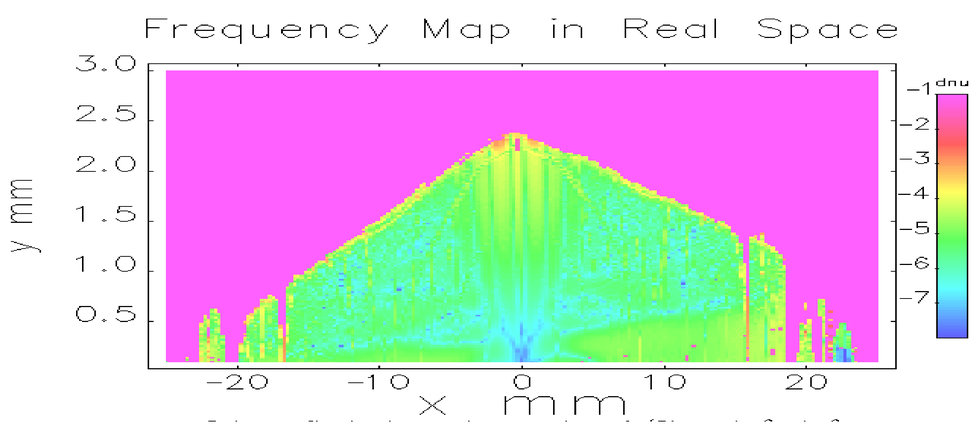

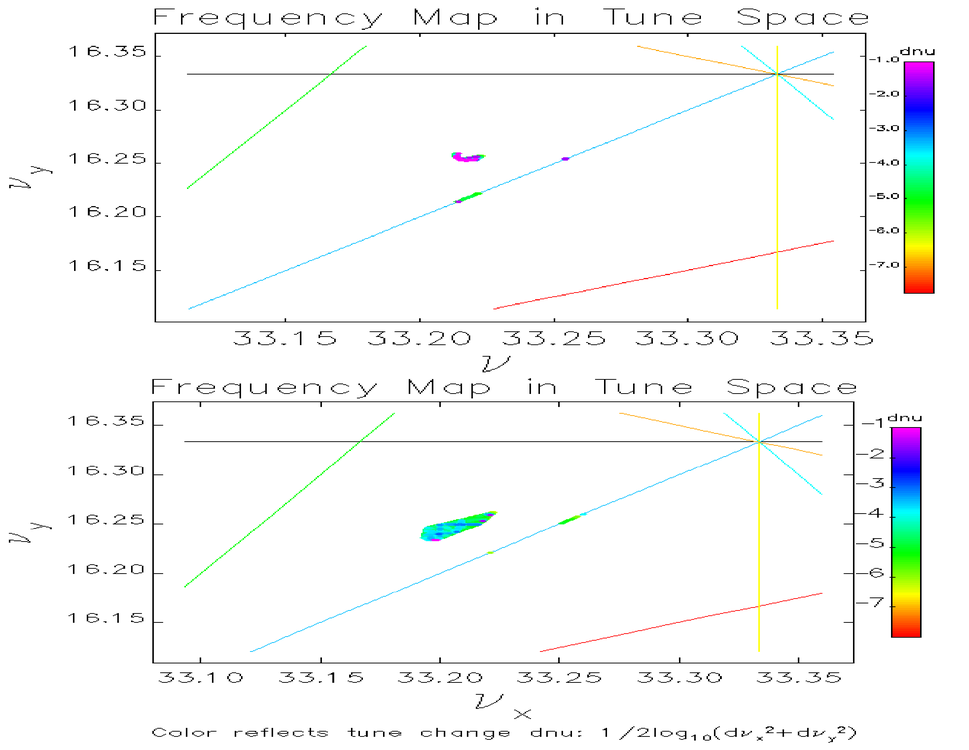

Upper: with 12 IDs, lower: bare lattice

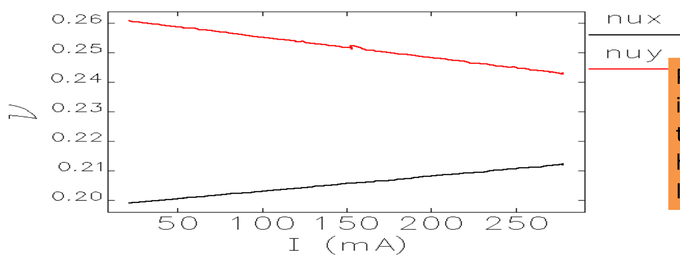

Problem: tune merges as the stored current increases. To separate the initial tunes so the working point remains at the nominal values has been proposed and will be implemented In the future.

Conclusion: On and off-momentum dynamic aperture are still acceptable and nonlinear re-optimization is not needed at this point.
Future work: Separate the tunes at operating high current.

Correction of ID-Induced Coupling

Y. Hidaka*, Y. Li, T. Shaftan, T. Tanabe, Y. Tian, G. Wang

BROOKHAVEN NATIONAL LABORATORY

*yhidaka@bnl.gov

Abstract: Large lifetime jumps have been occasionally observed since March 2016 at NSLS-II. These jumps were correlated with insertion device (ID) gap motions, particularly with one of the IVUs at Cell 17. This ID was found to have large localized skew quadrupole component variation with gap. As this issue prevents us from operating stably in the low-emittance mode, a global coupling feedforward system has been recently implemented and successfully deployed. Furthermore, the maximum gap limit has been reduced from 40 mm to 25 mm to limit the skew component variation during user operation. More local compensation is under consideration by introducing a new additional skew quadrupole near the problematic ID.

Local Skew Quad (from Hall Probe) @ Min. Gap

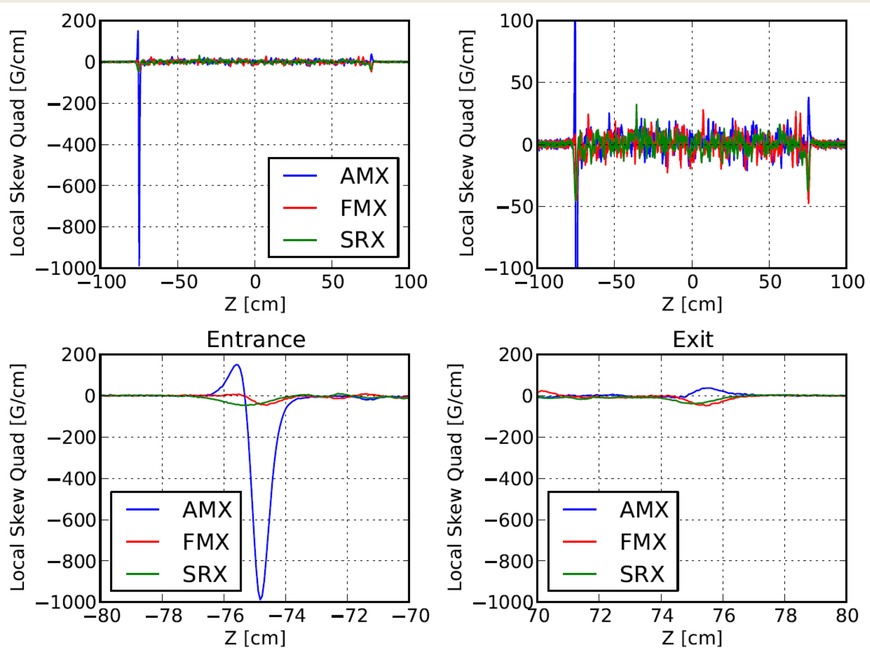

- Local skew quad error concentration @ AMX entrance (potentially from magic fingers)

Rotating Coil Measurements (Integrated Skew Quad vs. Gap)

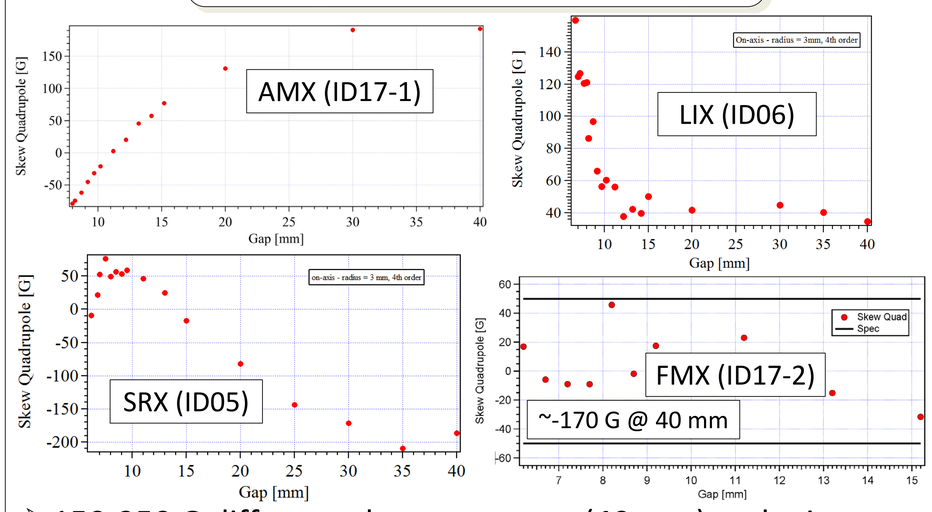

- 150-250 G difference between open (40 mm) and min. gap.
- SQ components are outside of ±50 G spec. above 15 mm gap.
- Open gap now set to 25 mm to reduce max SQ variation.

Beam-based ID Skew Quad Error Estimates

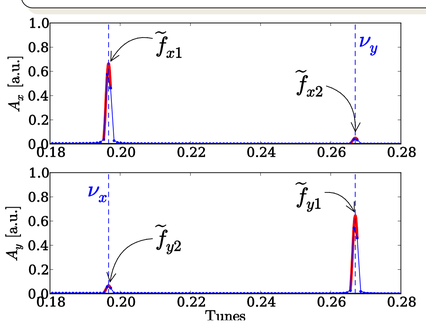

- Typical spectra of horiz. & vert. TbT data (Primary and secondary frequency components denoted by subscripts 1 & 2, respectively).
- Can fit ID SQ errors (along with normal quad errors and BPM gain/roll/deformation errors) based on RDT formula using new TbT-based lattice characterization algorithm called DTBLOC (Driving-Terms-Based Linear Optics Calibration) [See Y. Hidaka, et al., NAPAC 2016]

$$|f_{x1}| = \sqrt{2I_x\beta_{x0}}$$

$$|f_{y1}| = \sqrt{2I_y\beta_{y0}}$$

$$|f_{x2}| = \sqrt{2I_y\beta_{x0}}\sqrt{\left(2\Im\{f_{1001}\}+2\Im\{f^H_{1010}\}\right)^2+\left(2\Re\{f_{1001}\}-2\Re\{f^H_{1010}\}\right)^2}$$

$$|f_{y2}| = \sqrt{2I_x\beta_{y0}}\sqrt{\left(2\Im\{f_{0110}\}+2\Im\{f^V_{1010}\}\right)^2+\left(2\Re\{f_{0110}\}-2\Re\{f^V_{1010}\}\right)^2}$$

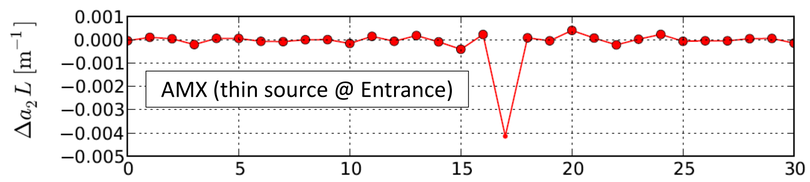

- AMX fits better (i.e. larger χ^2 reduction factor) if thin error source at entrance is assumed, which is consistent with the Hall probe measurement for AMX.
- SRX and FMX appear to have no strong localized error, as χ^2 reduction factors do not change much among thin and thick source assumptions.

$$f_{\substack{1001\\1010}}(s) \cong \frac{\sum_w (\Delta a_2 L)_w \sqrt{\beta_x^w \beta_y^w}\, e^{i\left(\Delta\phi_x^{w,s} \mp \Delta\phi_y^{w,s}\right)}}{4\left(1-e^{2\pi i(\nu_x \mp \nu_y)}\right)}$$

AMX (ID17-1) @ gap 6.4 mm	Integrated Skew Q [G]	χ^2 reduc. factor
Thin @ Entrance	**-578.3**	101.1
Thin @ Center	-958.1	80.7
Thin @ Exit	-1529.2	50.7
Thick (1.5 m)	-974.6	61.8

FMX (ID17-2) @ gap 6.4 mm	Integrated Skew Q [G]	χ^2 reduc. factor
Thin @ Entrance	-304.5	16.4
Thin @ Center	-197.8	17.8
Thin @ Exit	-118.6	17.6
Thick (1.5 m)	**-171.6**	17.3

SRX (ID05) @ gap 6.4 mm	Integrated Skew Q [G]	χ^2 reduc. factor
Thin @ Entrance	-76.6	25.5
Thin @ Center	-48.9	25.7
Thin @ Exit	-29.4	25.7
Thick (1.5 m)	**-44.4**	25.7

Global Coupling Feedforward System

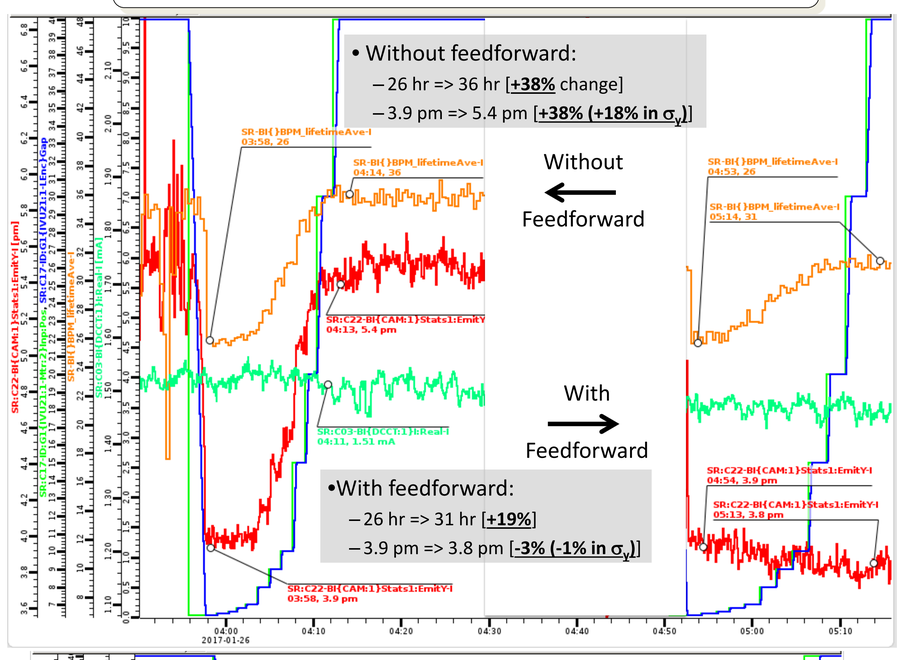

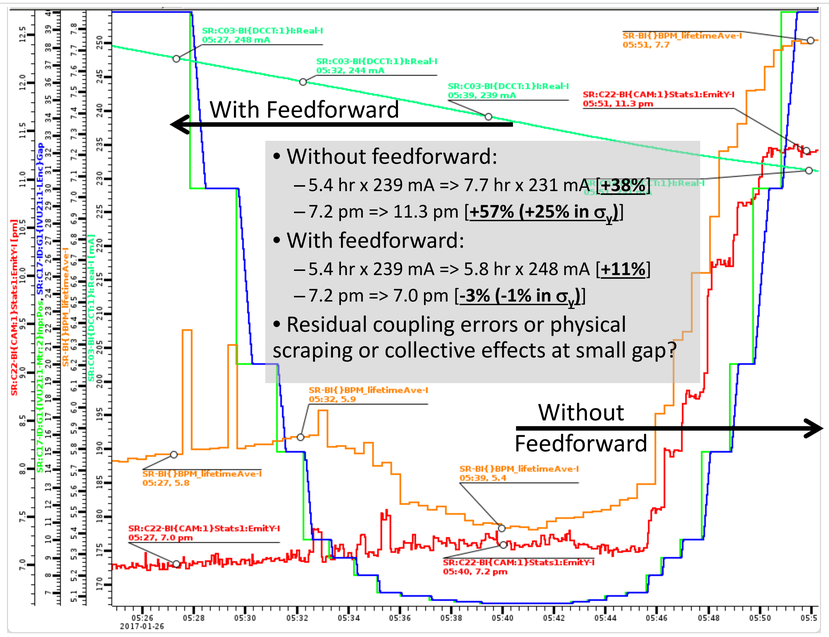

- Using existing 15 correction SQs in non-dispersive sections.
- Currently only corrects AMX (most offensive IVU), but can be extended to compensate SQ errors from other IDs.
- Took only 25 min. data acq. & 25 min. proc. to generate full 12-gap feedforward table.
- Max. 2A correction current (8×10^{-4} [m^{-1}] = 80 [G]).
- Reduced $\Delta\sigma_y$ of 25% to 1% in nominal operation condition
- Table generated for low current (2 mA) was equally effective at high current (250 mA)

Local Compensation Plan

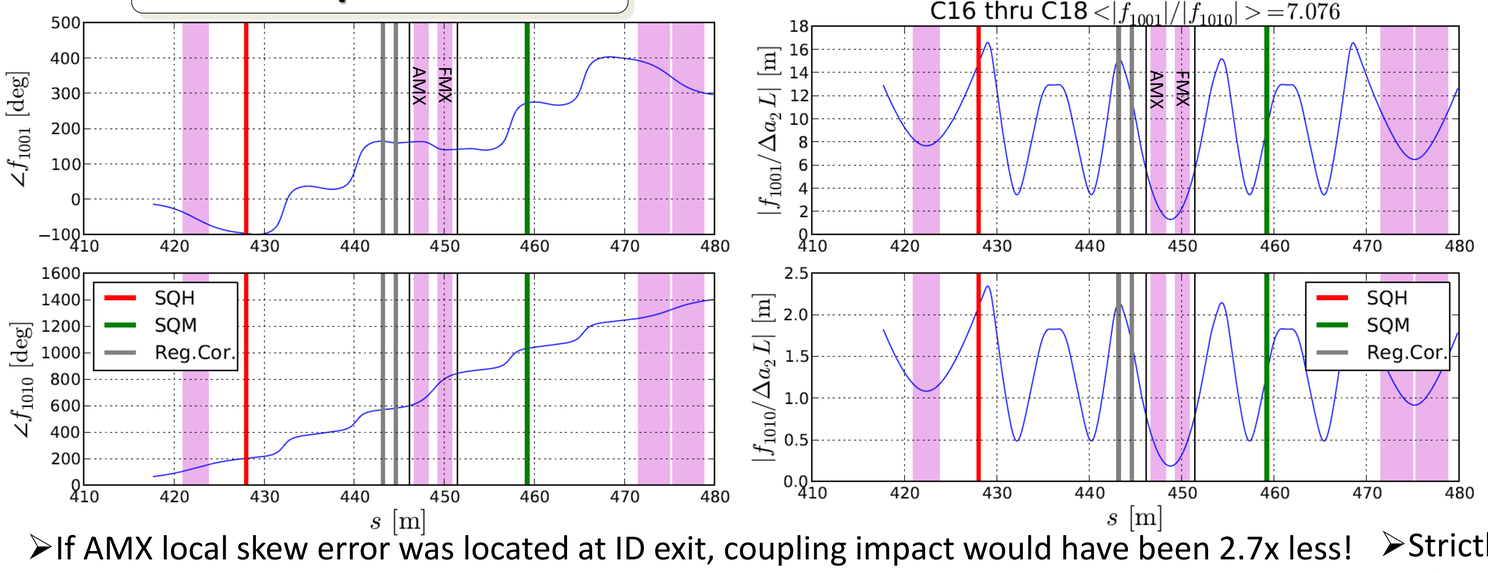

- If AMX local skew error was located at ID exit, coupling impact would have been 2.7x less!
- If we can add only one correction skew quad (SQ):
  - If f_{1001} phase at corr. SQ is within < 10° (or near 180°) from f_{1001} phase at ID SQ, good correction possible. Correction becomes hard for ~20°. and very ineffective for >~30°.
  - ID SQ errors in a short straight can be easily corrected within the same straight, as f_{1001} phase change is small, but this is not the case for ID SQ errors in a long straight.
- Strictly speaking we need 4 SQs to correct 1 SQ error source, but as diff. coupling effect dominates, 2 SQs at different phases are sufficient.
- During upcoming shutdown, we plan to add SQ components to C16-CL2, one of 2 slow orbit correctors (gray strips on plots) immediately upstream of AMX that have the right f_{1001} phases and large beta functions to compensate AMX-induced coupling locally.

NATIONAL SYNCHROTRON LIGHT SOURCE II

Lattice Characterization and Optimization at NSLS-II

Yongjun Li

Turn-by-Turn data

- From short bunch train excited by pinger
- From testing bunch train excited by bunch-by-bunch feedback

DC closed orbit

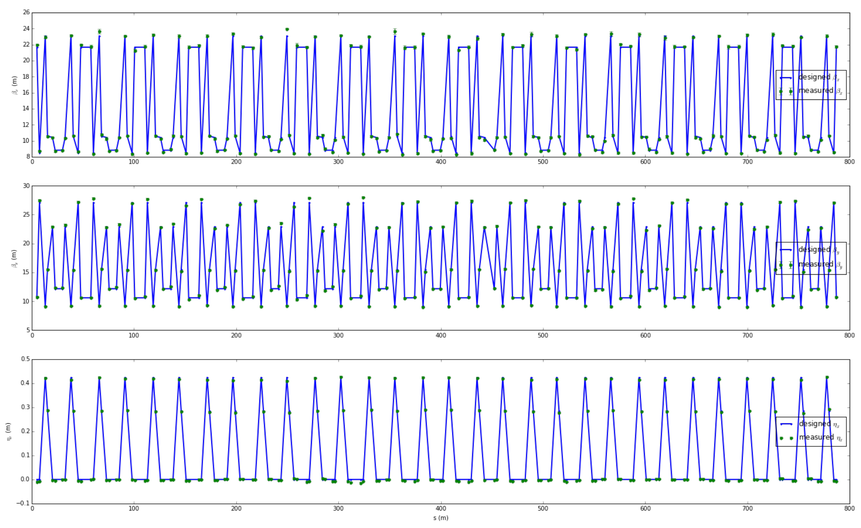

Beta-function and dispersion

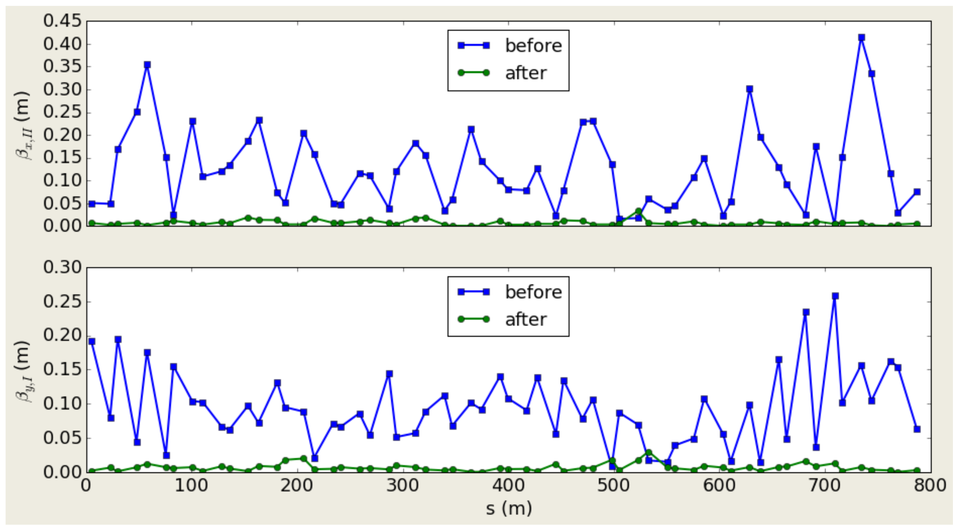

Coupled beta-function

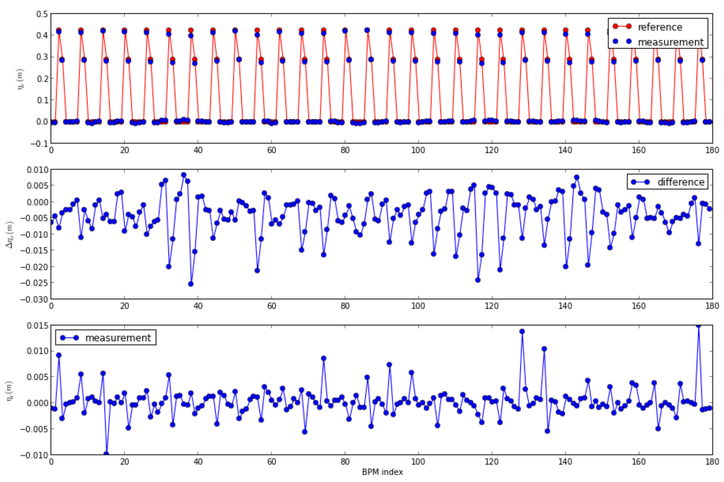

Residual H/V dispersion

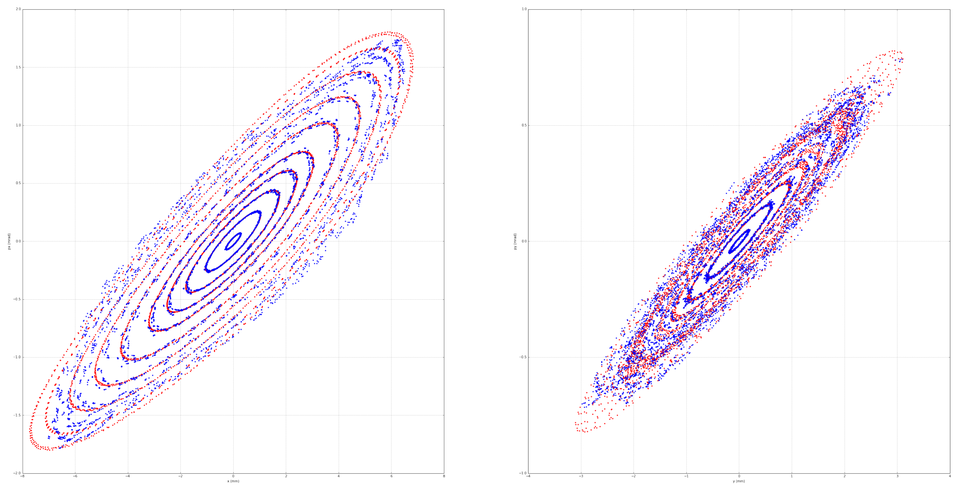

Phase space

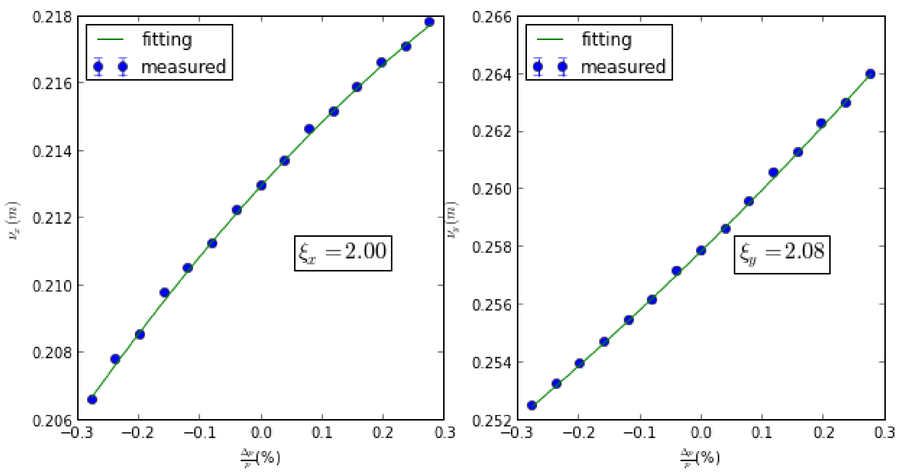

Chromaticity

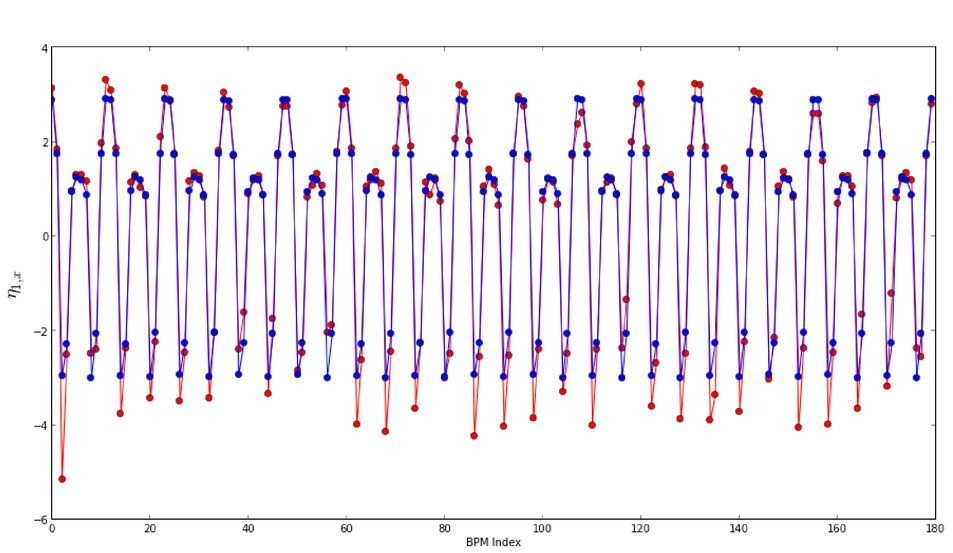

2nd order dispersion

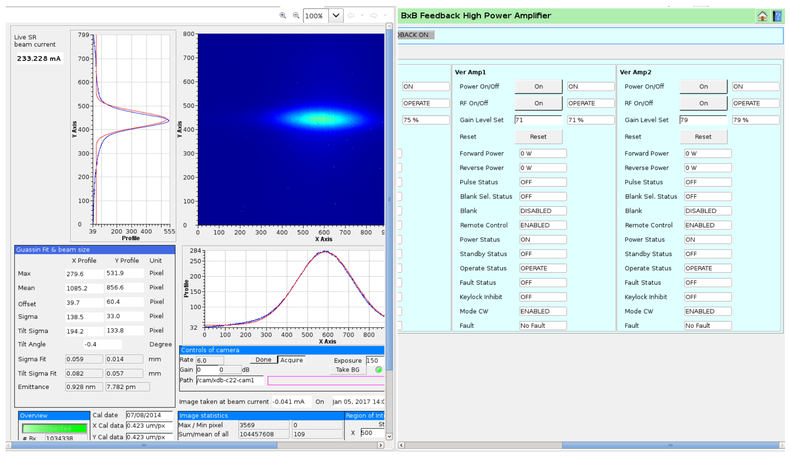

Optimize BxB feedback gain

Conclusion:

- SR lattice can be precisely characterized
- Iterative optimization was implemented

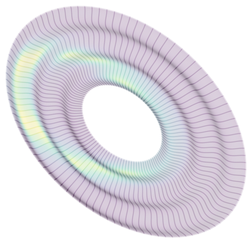

OSCARS

Open Source Code for Advanced Radiation Simulation

Dean Andrew Hidas
Brookhaven National Laboratory
dhidas@bnl.gov

BROOKHAVEN NATIONAL LABORATORY

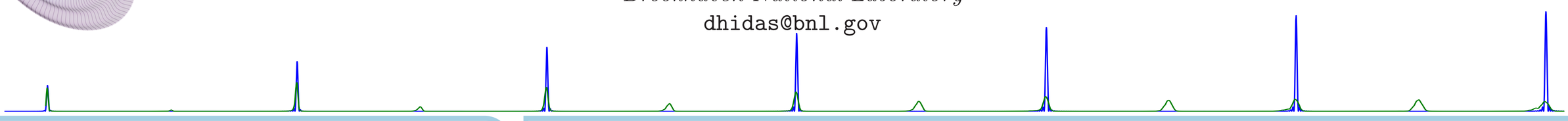

Introduction

Open Source Code for Advanced Radiation Simulation (OSCARS) [1] is an open source software developed at Brookhaven National Laboratory.

OSCARS is a general purpose code for the computation of radiation from charged particles in motion. Primary uses are for synchrotron and accelerator facilities where photon density distributions and heat loads on accelerator and beam-line equipment is of great interest. This software allows for the calculation of these properties on arbitrary shaped surfaces in 3 dimensions for arbitrary E&M field configurations in 3D.

Capabilities

With a simple and powerful user interface:

- Trajectories in E&M fields
- Calculation of Spectra, Flux, Power Density
- Arbitrary geometries in 3D
- Brightness calculations
- Multi-threaded, GPU, Grid/Cloud/OSG, and MPI capable

Trajectory

Particle trajectory calculations are done using a 4^{th}-order Runge-Kutta method. The equation of motion is the relativistic Lorentz equation given below where $\vec{p} = \gamma m_0 \vec{v}$

$$\frac{\mathrm{d}\vec{p}}{\mathrm{d}\tau} = q(\vec{E} + \vec{v} \times \vec{B}) \tag{1}$$

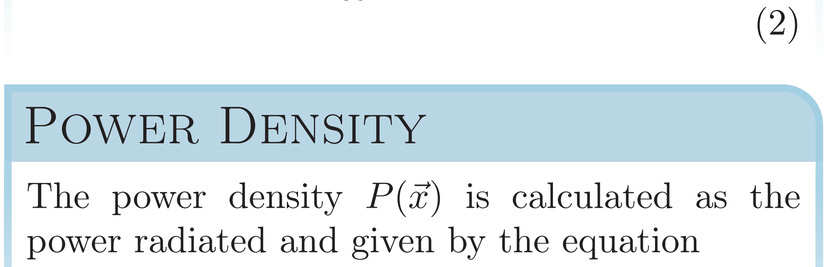

Flux Density

The spectrum and flux densities are calculated from the electric field in the frequency domain given in equation 2, which is derived from a Fourier transform of the Liéard-Wiechert potentials. It is valid in the near-field and for relativistic and non-relativistic particles alike. The field is calculated in all three spatial dimensions.

$$\vec{E}(\vec{r},\omega) = \frac{ie\omega}{4\pi c\epsilon_0}\int_{-\infty}^{+\infty} \frac{\vec{\beta} - \hat{n}(1+\frac{ic}{\omega D})}{D} e^{i\omega(\tau+\frac{D}{c})} d\tau \tag{2}$$

Power Density

The power density $P(\vec{x})$ is calculated as the power radiated and given by the equation

$$\frac{qI}{16\pi^2\epsilon_0 c}\int_{-\infty}^{\infty} \frac{\vec{n}\times((\vec{n}-\vec{\beta})\times\frac{\vec{a}}{c})}{(1-\vec{\beta}\cdot\vec{n})^5}\frac{1}{|\vec{r}|^2}(\hat{n}\cdot\hat{S})\,\mathrm{d}\tau$$

Work-flow

Easily define fields, particle beams, surfaces, and points in 3 dimensions in arbitrary directions, positions, and orientations. All computations can be run in single and multi-particle mode.

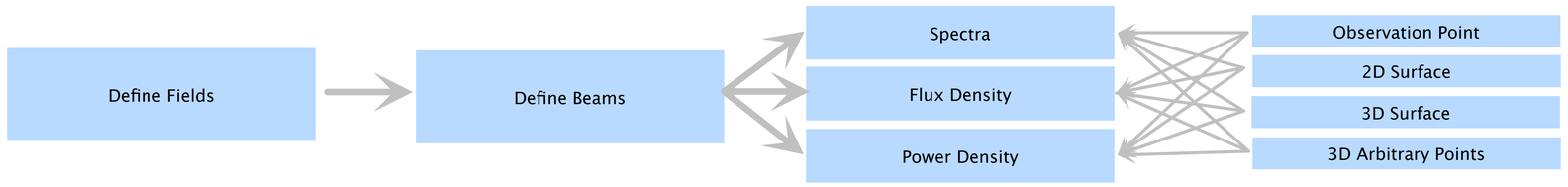

Fields	*Beams*	*Computations*	*Objects*
Dipole Fields	Allow multiple beams	Single-particle	Easy Translation
Gaussian Fields	Beam $\epsilon_{v,h}$ and $\beta_{v,h}$	Multi-particle	Easy Rotation
Undulators, Wigglers	Built-in particles	Mixed-particle	2D, 3D Surfaces
Any user function	User defined particle	MPI enabled	Arbitrary 3D Surfaces
3D Input files	Any direction	Grid compatible	Arbitrary 3D points

EXAMPLES

The following examples make use of a planar undulator U49 ($\lambda = 0.049$ [m], $B_{\max} = 1$ [T]) and a similar elliptically polarizing undulator (EPU49) with B_v and B_h phase shifted by $\phi = \pi/2$.

The beam parameters are similar to the NSLS-II 6.6 [m] straight with $\epsilon_v = 0.008$ [nm rad], $\epsilon_h = 0.9$ [nm rad], $\beta_v = 0.8$ [m], $\beta_h = 1.5$ [m], $E = 3$ [GeV], and $\Delta E/E = 0.001$, pointing in the $+\hat{z}$ direction.

Power Density 3D

OSCARS is capable of calculating power density distributions on arbitrary geometries in 3D. Shown below is the power density distribution from the example EPU49 as seen on a corrugated and tapered beam-pipe (*bottom*).

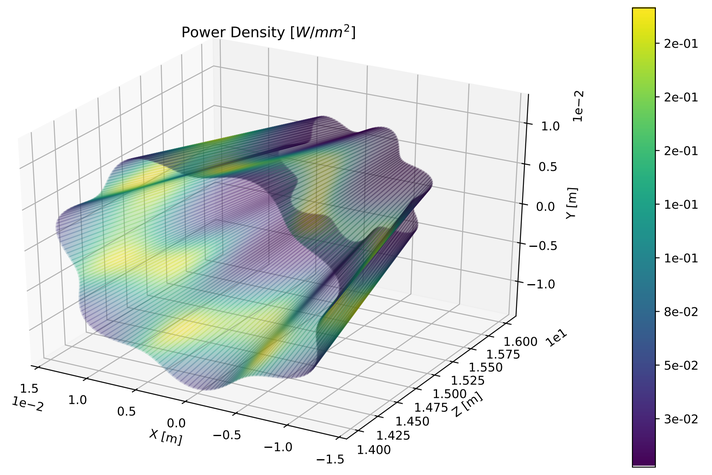

Spectra

The following is an example of the single-electron and multiple-electron spectra from U49.

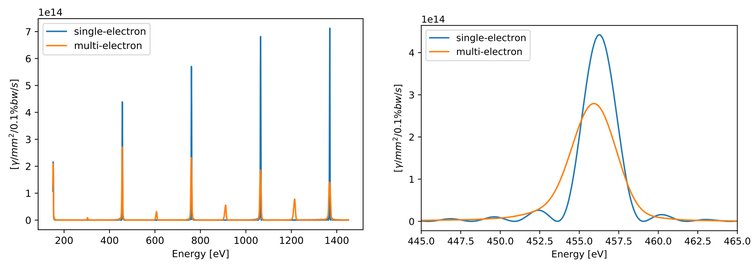

Undulator Brightness

Example brightness calculation for U49 for the first 8 odd harmonics. Here the maximum K value is 4.88 (corresponding to a field of 1.0 [T]).

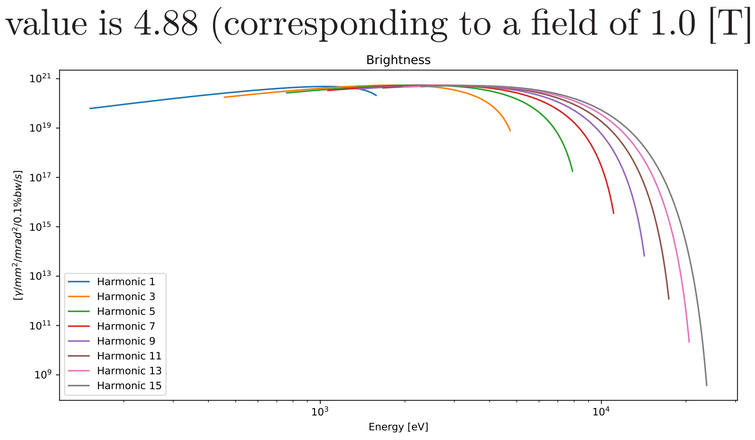

Flux

Below is an example flux calculation for the example U49 for single-particle (*left*) and multi-particle (*right*) simulations at $E = 456$ [eV].

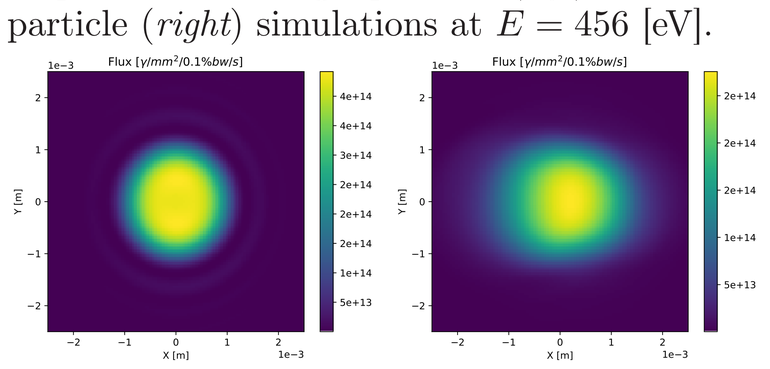

Power Density

This is an example of the power density calculated 30 [m] downstream of the example EPU49 on a flat surface perpendicular (*left*) and parallel (*right*) to the beam direction.

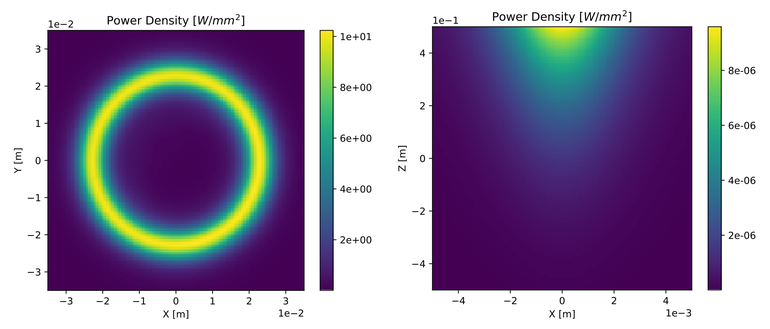

Conclusions

A simulation code for advanced radiation simulation has been developed which is fast, powerful, flexible, and open source. Notably, this new simulation is capable of calculating power densities on arbitrary geometries in 3D.

See More

[1] http://oscars.bnl.gov

Acknowledgments

Supported by the U.S. Department of Energy under contract DE-AC02-98CH10886.

Novel Accelerator Physics Measurements Enabled by NSLS-II RF BPM Receivers

Boris Podobedov, Weixing Cheng, Yoshi Hidaka

BROOKHAVEN NATIONAL LABORATORY

NATIONAL SYNCHROTRON LIGHT SOURCE II

Motivation for New BPM Capability: Resolving Several Bunches within One Turn

- Why single- or few bunch fills?
  - For various beam dynamics studies, especially
    - 1) single bunch collective effects, incl. impedance measurement
    - 2) single particle non-linear dynamics
    - 3) beam lifetime and instability diagnostics
- Why resolution improvement is beneficial for these?
  - Measurements are very sensitive (effects are small, and could be masked by machine drifts)
  - Need to be done at low currents
- Apart from resolution why special BPM signal processing?
  - To provide "bunch-by-bunch capability"* for overcoming the machine drifts

* For at least a few, well separated, bunches

Motivation Example: Transverse Impedance Measurement

- What is the impedance (or kick factor) of an accelerator component, i.e. an insertion device chamber?
- By design, these are small.
- Impedance is not directly measured, but Z-related effects ~Q_b are.
- Take Q_b=1 nC, β_y=3 m, k_y=500 V/pC/m
  - Tune shift ~4×10^{-5}
  - Closed orbit shift ~0.7 μm rms per Δy=1 mm
- These are hard to measure!
- The standard approach, via multiple injections or time-decay, is virtually impossible due to "machine drifts"
  - typically at low current and no fdbk.: tune jitter >10^{-4}, rms orbit drift >1 μm/min
- Can be overcome by the relative measurements, with high-Q_b and low-Q_b bunches

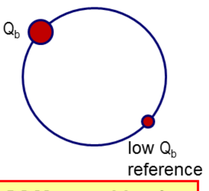

Need good resolution at low current, and many BPMs capable of resolving the orbits of at least two bunches

From Accurately Measured Tune Difference to Coupling Impedance

Kick factor definition, relation to effective coupling impedance and measurement via tuneshift with current:

$$< x' >= \frac{Q_b}{E/e} k_{kick} < x_0 >$$

$$k_{kick} \propto \int |\tilde{\rho}|^2 \, \mathrm{Im}[Z_x(\omega)] d\omega$$

$$\delta\nu(Q_b) = -k_{kick} Q_b \frac{< \beta_x >}{4\pi E/e}$$

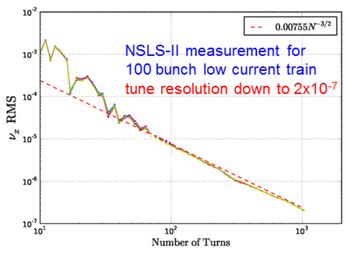

resolve tunes to 10^{-6}

$$\delta k_{kick} = 4\pi\delta(\nu_{lowQ_b} - \nu_{hiQ_b}) \frac{E/e}{\Delta Q_b < \beta_x >}$$

get kick factors as low as 10 V/pC/m*

*assumed 1 nC, β=4 m, 3 GeV, σ=20 ps

=> Equivalent to the impedance from ø = 5 mm Cu pipe of only 10 cm long*

Unequal Charge Bunches Kicked with a Pinger

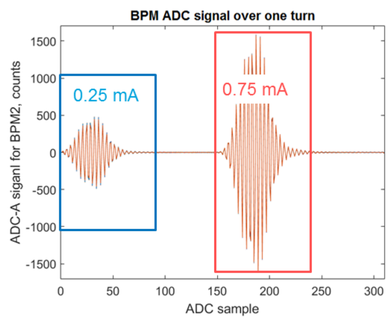

- Two bunch fill with unequal bunches
- Pinger timing adjusted for equal vertical kick
- ADC data processed to get separate TbTs for each bunch

Turn-by-Turn Signals

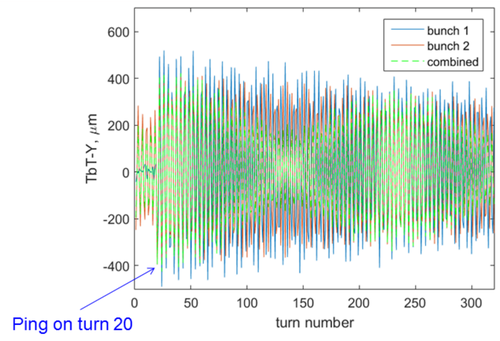

- Each bunch decays a long time, but the combined shows beating
- Also instability for high current bunch before the ping

Tunes are Distinctly Different

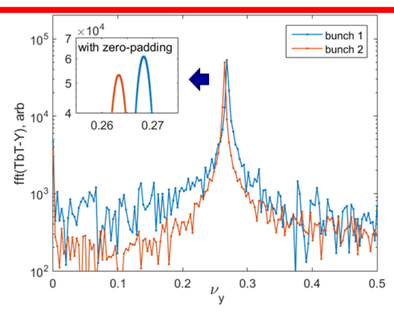

- Single BPM FFT shows tunes are clearly unequal
- Detailed analysis with interp'd FFT for 180 BPMs gives
  ν_y=0.26833 ±1.93e-5 (bunch 1) and ν_y=0.26334 ± 6.90e-6 (bunch 2)
- Tune difference of 5e-3/(0.5 mA) is consistent with other measurements

Same Measurement in the Horizontal

- Same two bunches, 0.25 mA (1) and 0.75 ma (2), use hor. pinger
- ADC data processed to get separate TbTs for each bunch

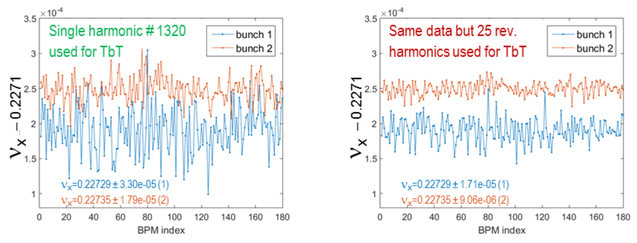

$\Delta\nu_{21}$ = (6.0 ± 3.8)*1e-5 ⇒ $\Delta\nu_{21}$=(6.0 ± 1.9)*1e-5

- Resolution improvement (est. x4) has helped; now convincingly show that hor. tune goes up with current (i.e. total wake is slightly focussing).

Local Impedance Measurement: Vertical Scraper

- Measure tune difference between low- and high-Q bunches
- Repeat with the scraper inserted
- Change in the tune difference is due to (added) scraper impedance
- 1.4 mA 100 bucket train (reference) + 0.3 mA camshaft ½ ring away

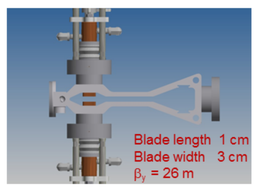

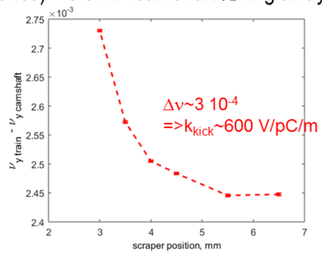

- Complimentary measurement would be from closed orbits (no kick), TBD

Horizontal Scraper

- Two bunches stored, inner blade moved in
- Change in the tune difference is due to (added) scraper impedance

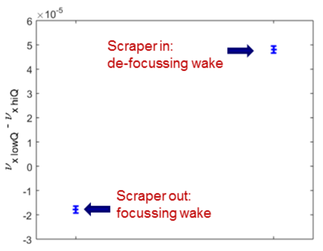

- With scraper blade close to the beam, tune-current slope changes to negative (agrees with expectation)

Measure Low-β Insertion Device Chamber

- Example of a fixed impedance component, use local bumps to probe Z
- Cell 21 has two EPUs (out-of-vacuum)
- Vacuum chamber is Al pipe, 4.8 m length, β_{y0}=1.2 m, resistive wall is expected to dominate, RW kick factor 56 V/pC/m at σ_τ(0.3mA)=16.2 ps measured separately

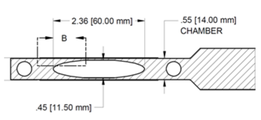

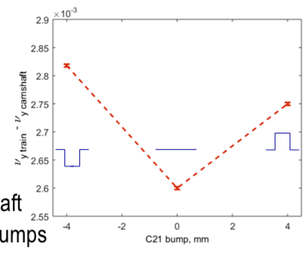

- Injected 1.4 mA train + 0.3 mA camshaft
- Camshaft decayed some during the bumps
- Measured kick factor of 210 V/pC/m tune is about x4 higher than the theory for Al but is likely due to NEG coating

Synchrotron Tune Shift with Current

- RF cavity feedforward provides short (<1/f_s) RF amplitude jump
- Beam (3 bunches, 1/3 ring apart each) is kicked longitudinally, synchrotron tune detected on dispersive BPMs (60 total)

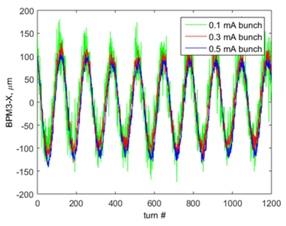

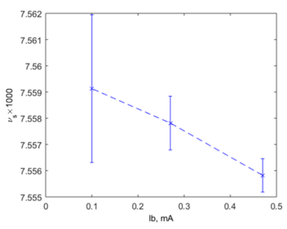

- As expected, tune change is tiny (imperfect cancellation of coherent and incoherent tune shifts), yet measurable, ~ 10^{-5}/mA with this method.
- Detecting signals around 2 f_s should provide longitudinal impedance

Single Shot Measurement of Tune Shift With Amplitude

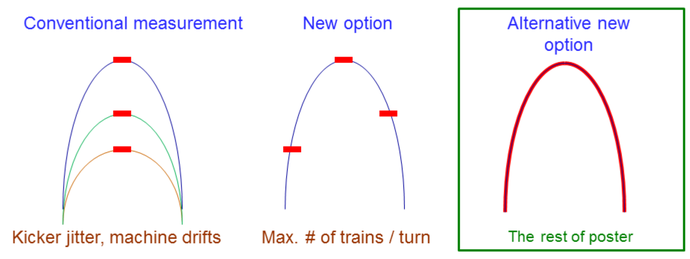

Measurement Setup and Sample Data

- Fairly uniform fill pattern at low current (no collective effects !)

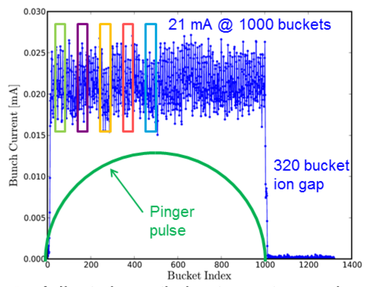

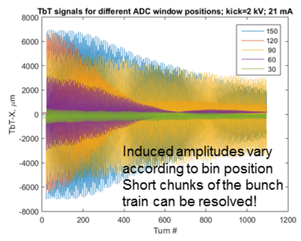

- Adjust pinger timing to center maximum kick in the middle
- 11 sample wide ADC window (~47 RF buckets); slide over the turn
- Results independent of window width when it's << kicker rise time

Final Results: Horizontal

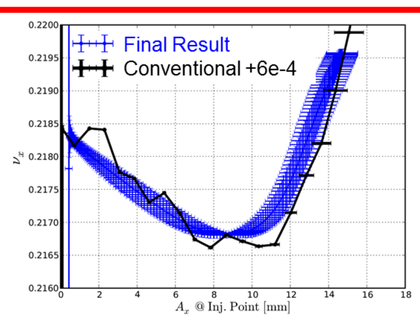

- Final result for 5mA/1000 bunches, single pulse of 2 kV
- Conventional measurement: 2 mA/100 bunches; 20 separate "pings"; clear pulse-to-pulse jitter, longer term drifts are likely
- Further optimization of new technique possible

Conclusions and Future Plans

- Single-bunch resolution of NSLS-II BPMs was recently improved by an order of magnitude to about one micron TbT at ~1 nC/bunch. Plus we can now resolve TbT signals from several bunches stored in the ring.
- Having this capability on all NSLS-II RF BPMs is extremely valuable for sensitive collective effect or single particle dynamics measurements. It allows us to simultaneously measure bunches with different charges (or kick amplitudes) thus eliminating harmful effects of machine drifts.
- We presented some novel accelerator physics measurements enabled by these new BPM capabilities. These include a new technique of probing the ring impedance, single-shot tune shifts with amplitude, etc.
- BPM ADC processing is presently done off-line but is being implemented in FPGA, so that improved resolution, and multi-bunch capability will be available in real time.
- Contributions from Kiman Ha, Joe Mead, Om Singh, Dmitri Teytelman and Kurt Vetter are greatly acknowledged.

Experimental Crosscheck of Algorithms for Magnet Lattice Correction

V. Smaluk, X. Yang, W. Guo, Y. Hidaka, G. Wang, Y. Li, L. Yang

BROOKHAVEN NATIONAL LABORATORY

NATIONAL SYNCHROTRON LIGHT SOURCE II

Abstract

Performance, capabilities and limitations of various algorithms for linear magnet optics correction have been studied experimentally at NSLS-II. For the crosscheck, we have selected 4 algorithms based on turn-by-turn beam position analysis: weighted correction of betatron phase and amplitude, independent component analysis, model-independent analysis, and driving-terms-based linear optics characterization. A LOCO algorithm based on closed orbit measurement has been used as a reference. For the correction, either iterative solving of linear problem (matrix inversion with singular-value decomposition) or variational optimization has been used. For all the algorithms, accuracy limitations and convergence of linear lattice correction are discussed.

LOCO

- Linear Optics from Closed Orbits (LOCO) was established at NSLS [4].
- The orbit response matrix is measured by beam position monitors (BPMs).
- Measured data is fitted to a lattice model. Fit parameters: quadrupole (normal and skew) strengths, BPM gains and rolls, corrector gains and rolls.
- The Matlab-based LOCO code [5] implemented at NSLS-II [1] is used as a reference for crosscheck of algorithms based on turn-by-turn BPM data.

Betatron Phase and Amplitude Correction

- Spectral analysis of turn-by-turn BPM data provides high-precision measurement of the frequency, amplitude and phase of betatron oscillation. Both amplitude and phase can be used for lattice correction, either independently or in combination with certain weight factors.
- A linear equation is solved for the lattice correction, the response matrix is calculated using the design model.
- The optics analysis and correction using turn-by-turn BPM data has been implemented at NSLS-II during the machine commissioning [2, 3].
- Here we have compared two options: using phase only and using weighted amplitude and phase.

Independent Component Analysis

- ICA method [6,7] has been developed for simultaneous linear optics and coupling correction using turn-by-turn BPM data.
- The amplitudes and phases of the projection of the normal modes on the horizontal and vertical BPMs are extracted from turn-by-turn data.
- Measured data is fitted to a lattice model, the fitting scheme is similar to the LOCO algorithm [2].

Driving-Terms-Based Linear Optics Characterization

- DTBLOC algorithm [8] has been recently developed to characterize the linear optics from turn-by-turn data, based on the resonance driving terms (RDTs) for beta-beat and linear coupling [9].
- Turn-by-turn data + dispersion from all BPMs around the ring. The real and imaginary parts (or, amplitude and phase) of two frequency components in each plane are extracted by interpolated FFT with windowing.
- Measured data is fitted to a lattice model. The fitting parameters: quadrupole (normal and skew) strengths, BPM errors.
- The fitting values are estimated via SVD using a Jacobian matrix with analytical expressions based on RDTs.

Model-Independent Analysis

- Model-independent analysis (MIA) was originally proposed for BPM data processing at Stanford linear accelerator [10].
- For circular accelerators, MIA is a statistical analysis of turn-by-turn BPM data using singular-value decomposition (SVD). This approach uses SVD but it does not require a lattice model.
- The turn-by-turn beam position measured by M BPMs during N turns is presented as a $M \times N$ matrix **B**. MIA is performed by SVD of the matrix **B** decomposing the motion into a set of temporal modes and spatial modes. The spatial mode represents the variation of the temporal mode along the ring.
- A lattice correction code based on MIA has been developed at NSLS-II [11].

Experimental Data

- Test lattice with large beta beats (adding random errors to the quadrupoles).
- This lattice is the initial one to be corrected by every algorithm.
- Beta functions and betatron phases have been obtained by spectral analysis of turn-by-turn BPM data using FFT refinement algorithms.
- The BPM offset and roll errors obtained from LOCO have been taken into account.

Residual errors (r.m.s., 3 iterations).

Algorithm	$\Delta\beta_x/\beta_x$ %	$\Delta\beta_y/\beta_y$ %	$\Delta\psi_x$ °	$\Delta\psi_y$ °	$\Delta\eta_x$ mm	η_y mm
no corr.	8	10	4.5	3.5	18	8
LOCO	2.1	1.4	0.5	0.2	2.6	4.4
phase only[1]	2.3	1.8	0.6	0.5	39	9.9
phase&amp.[1]	2.8	1.7	0.7	0.9	11	7.8
ICA	2.6	1.6	0.5	0.4	5.0	2.3
MIA	2.8	1.7	0.7	1.0	5.4	6.8
DTBLOC	3.0	1.9	0.4	0.8	2.3	4.5

[1] no dispersion corrected

Beta beats before and after correction.

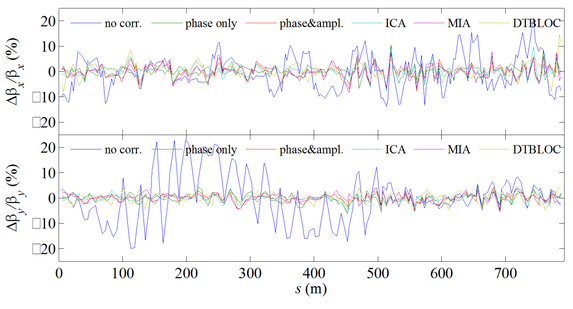

Phase errors before and after correction.

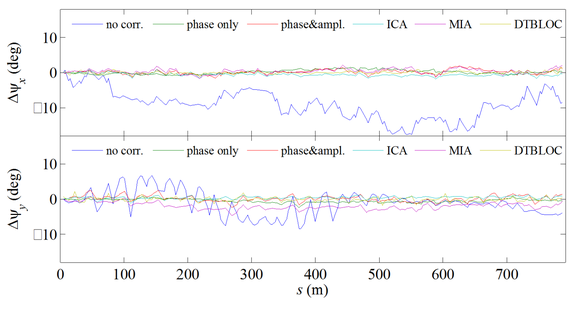

Convergence

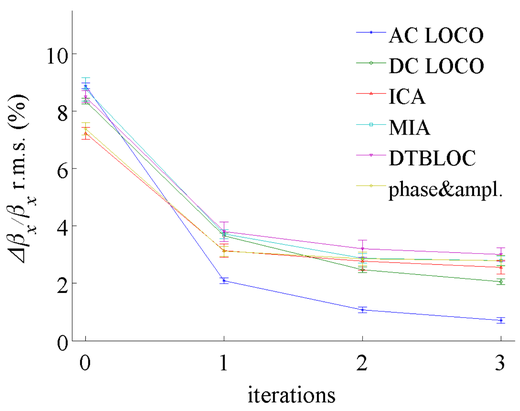

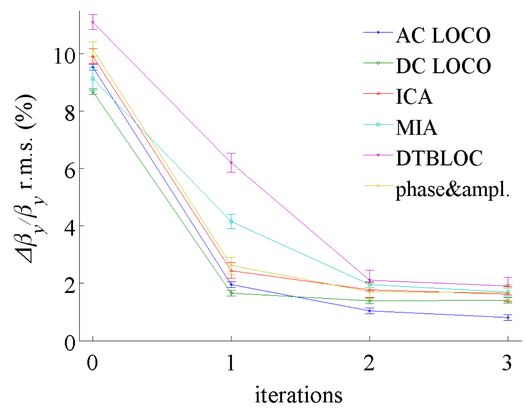

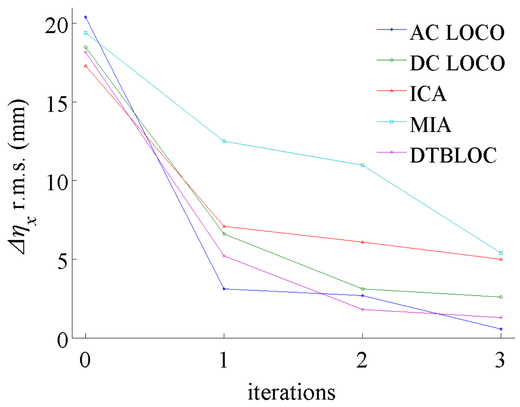

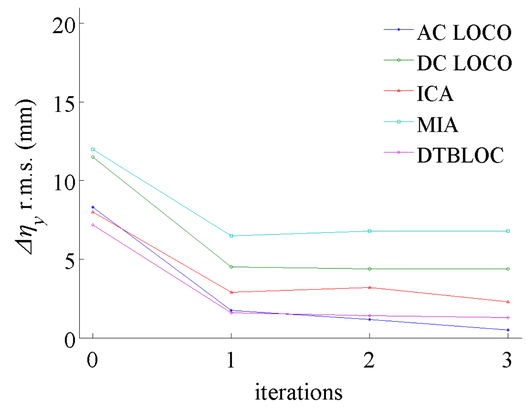

References

[1] T. Shaftan, "NSLS-II Accelerator Commissioning and Transition to Operations", WEPOY055, this conference.

[2] G.M. Wang, T. Shaftan, F. Willeke *et al.*, "NSLS II Commissioning report", BNL Tech. Note 168, 2015.

[3] Y. Li, L. Yang, W. Cheng, "Using Big Data in NSLS-II Storage Ring Commissioning", *ICAP'15*, Shanghai, 2015.

[4] J. Safranek, "Experimental determination of storage ring optics using closed orbit response measurements", *Nucl. Instr. Meth.*, A388, p. 27, 1997.

[5] J. Safranek, G. Portmann, A. Terebilo, C. Steier, "MATLAB-based LOCO", in *Proc. EPAC'02*, Paris, 2002.

[6] X. Huang, S. Y. Lee, E. Prebys, R. Tomlin, "Application of independent component analysis to Fermilab booster", *PRSTAB*, vol. 8, p. 064001, 2005.

[7] X. Huang, X. Yang, "Linear Optics and Coupling Correction with Turn-by-turn BPM Data", *IPAC'15*, Richmond, 2015.

[8] Y. Hidaka, B. Podobedov, J. Bengtsson, "Linear optics characterization and correction method using turn-by-turn BPM data based on resonance driving terms with simultaneous BPM calibration capability", NAPAC'16, Chicago, 2016.

[9] A. Franchi *et al.*, "Vertical emittance reduction and preservation in electron storage ring via resonance driving terms correction", *PRSTAB*, vol. 14, p. 034002, 2011.

[10] J. Irwin, C. X. Wang, Y. T. Yan *et al.*, "Model-Independent Beam Dynamics Analysis", *PRL* 82, no. 8, p. 1684, 1999.

[11] Y. Li, private communication, 2015.

NSLS-II Insertion Devices

T. Tanabe*, Y. Hidaka, D. Hidas, J. Rank, P. Cappadoro, H. Fernandes, D. A. Harder, M. Musardo, T. Corwin, C. Rhein and W. Liccardi

*ttanabe@bnl.gov

BROOKHAVEN NATIONAL LABORATORY

NATIONAL SYNCHROTRON LIGHT SOURCE II

NSLS-II Insertion Device List (NSLS-II Project)

Table 1: Insertion Devices planned as of 02/19/15

Beam Line	Type	Design	Beam port	Location	Length [m]	Period [mm]	Peak Field [T]	K_{max}	Canting Angle [mrad]	Vac Aper [mm]	Fund. [eV]	Total Power [kW]
CSX1 /CSX2	EPU49	PPM	Low-β_x	23-ID	4 (2×2)	49	0.57 (heli) 0.94 (Lin) 0.72 (vlin) 0.41 (45d)	2.6 (heli) 4.3 (Lin) 3.2 (vlin) 1.8 (45d)	0.16	8.0	230 (heli) 180 (Lin) 285 (vlin) 400 (45d)	7.3 (heli) 9.9 (Lin) 5.5 (vlin) 1.7 (45d)
IXS	IVU22	Hybrid	High-β_x	10-ID	6 (1×3) center	22	1.52	1.52	0	7.2	1802	4.7x2
HXN	IVU20	Hybrid	Low-β_x	3-ID	3	20	1.03	1.83	0	5.0	1620	8.0
CHX	IVU20	Hybrid	Low-β_x	11-ID	3	20	1.03	1.83	0	5.0	1620	8.0
SRX /(XFN)	IVU21	Hybrid	Low-β_x	5-ID	1.5 downstream	21	0.90	1.79	2.0	6.2	1570	3.6
XPD /PDF	DW100	Hybrid	High-β_x	28-ID	6.8 (2×3.4)	100	1.8	~16.5		11.5		64.5

NSLS-II Insertion Device List (NEXT, ABBIX, Partner)

Table 1: Insertion Devices planned as of 02/19/15

Beam Line	Project	Type	Design	Beamport	Location	Length [m]	Period [mm]	Peak Field [T]	K_{max}	Canting Angle [mrad]	Vac Aper [mm]	Total Power [kW]
ESM	NEXT	EPU105/ EPU57	PPM	Low-β_x	21-ID	2.7/1.4	105/49	0.74/0.57 (heli) 0.90 (vlin) 1.14/0.83 (Lin)	7.23/3.55 (heli) 7.23/3.06(vlin) 11.2/4.4 (Lin)	2.0		4.22/1.2 (heli) 4.22/0.86 (vlin) 10.1/2.0 (Lin)
SIX	NEXT	EPU57	PPM	High-β_x	2-ID	7.0 (2×3.5)	57	0.57 (heli) 0.83 (Lin)	3.55 (heli) 4.41 (Lin)	0		4.4 (heli) x2 6.8 (Lin) x2
ISR	NEXT	IVU23	Hybrid	High-β_x	4-ID	2.8	23	0.95	2.05	2.0	6.0	
SMI	NEXT	IVU23	Hybrid	High-βx	12-ID	2.8	23	0.95	2.05	2.0	6.0	
ISS+XFP	NEXT	DW100	Hybrid	High-β_x	18-ID	6.8 (2×3.4)	100		~16.5		11.5	64.5
FXI	NEXT	DW100	Hybrid	High-β_x	8-ID	6.8 (2×3.4)	100		~16.5		11.5	64.5
LIX	ABBIX	IVU23	Hybrid	High-β_x	16-ID	2.8	23	1.02	2.2	0	5.5	
FMX/AMX	ABBIX	IVU21	Hybrid	Low-β_x	17-ID	1.5 x 2	21	0.90	1.79	2.0	6.2	3.6
SST	Partner	U42	Hybrid	Low-β_x	7-ID	1.6	42	0.82	3.27	2.0	8.0	3.2
	Partner	EPU60	PPM	Low-β_x	7-ID	0.89	60	0.73 (heli) 1.02 (Lin)	4.1 (heli) 5.7 (Lin)		8.0	1.8 (heli) 2.7 (Lin)
NYX	Partner	IVU18	Hybrid	Low-β_x	19-ID	1.0	18	0.95	1.55	0	5.4	2.5
HEX	Partner	SCW55	EM	Low-β_x	27-ID?	1.0	55	4.2	21.6	0	10	49.7

Existing Beamlines and Their Timeline

Cell Number	ID name	BL name	ID params	ID install date	BL first light date
NSLS-II Project					
C23 (canted)	EPU-2	CSX-1	2m-EPU49	Aug. 2014	Oct. 2014
C23 (canted)	EPU-1	CSX-2	2m-EPU49	Aug. 2014	Jan. 2016
C3	IVU	HXN	3m-IVU20	June. 2014	Nov. 2014
C5	IVU	SRX	1.5m-IVU21	June. 2014	Dec. 2014
C10	IVU	IXS	3m-IVU22	Aug. 2014	Nov. 2014
C11	IVU	CHX	3m-IVU20	June. 2014	Nov. 2014
C28	DW	XPD	6.8m-DW100	Aug. 2013	Nov. 2014
ABBIX					
C16	IVU	LIX	2.8m-IVU23	May. 2015	Aug. 2015
C17 (canted)	IVU	AMX	1.5m-IVU21	May. 2015	Mar. 2016
C17 (canted)	IVU	FMX	1.5m-IVU21	May. 2015	Mar. 2016
NEXT					
C4 (canted)	IVU	ISR	2.8m-IVU23	Sep. 2015	July. 2016
C8	DW	ISS	6.8m-DW100	Oct. 2013	Apr. 2016
C12 (canted)	IVU	SMI	2.8m-IVU23	Dec. 2015	Nov. 2016
C21	EPU57	ESM	1.4m-EPU57	Apr. 2016	July. 2016
C21	EPU105	ESM	2.7m-EPU105	Dec. 2016	
C2	EPU	SIX	3.5m-EPU57	Aug. 2016	Feb. 2017
BDN & Partner					
C8	Dipole	TES			Aug. 2016
C11	3PW	CMS		May. 2016	Aug. 2016
C19 (canted)	IVU	NYX	1m-IVU18	Aug. 2016	Nov. 2016
C17	3PW	XFP		May. 2016	July. 2016
C18	DW	FXI	6.8m-DW100	Nov. 2013	

3.4-m Damping Wiggler (1.8T)

Novel Four-Array APPLE-II (EPU49)

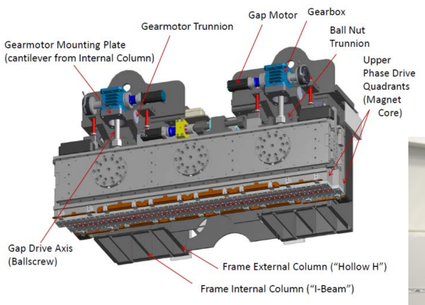

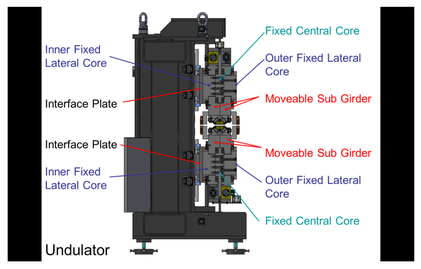

In-Vacuum Undulator with Side Window and Differential Adjuster

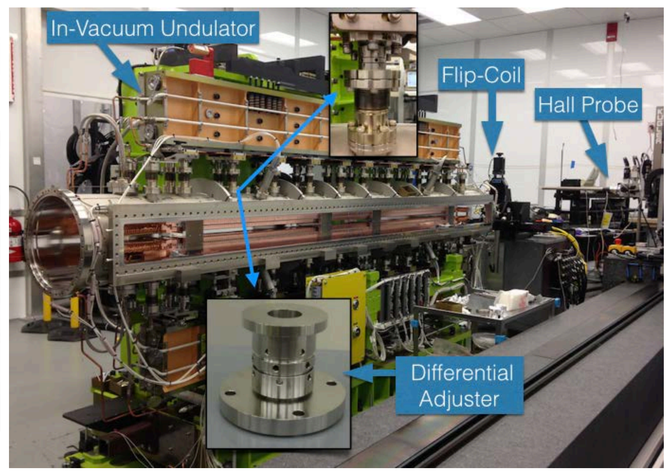

3-m IVU-U20

1.5-m IVU-U21 (Canted)

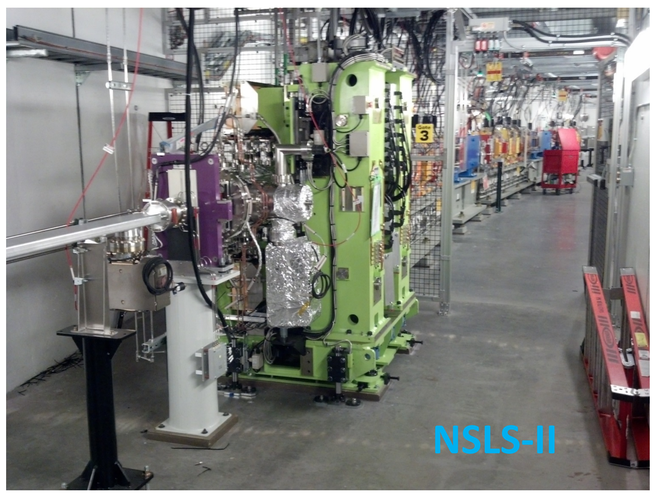

Two 1.5-m IVU-U21 (Canted)

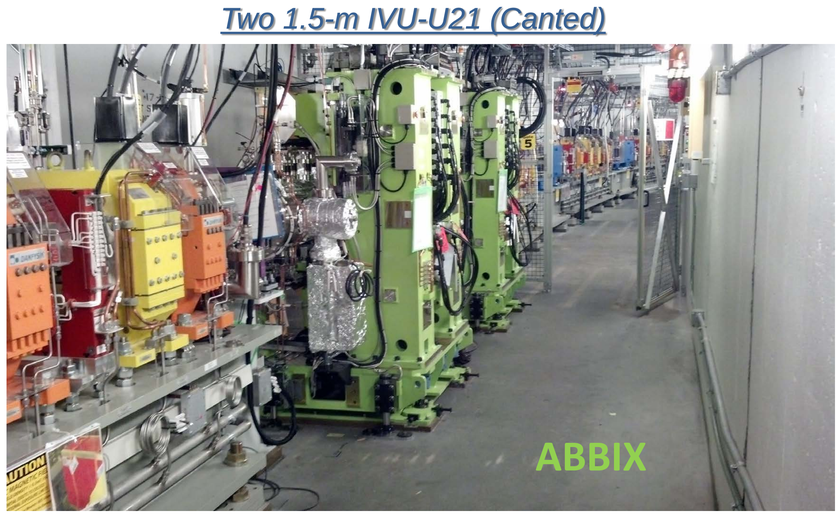

2.8-m IVU-U23 for LIX

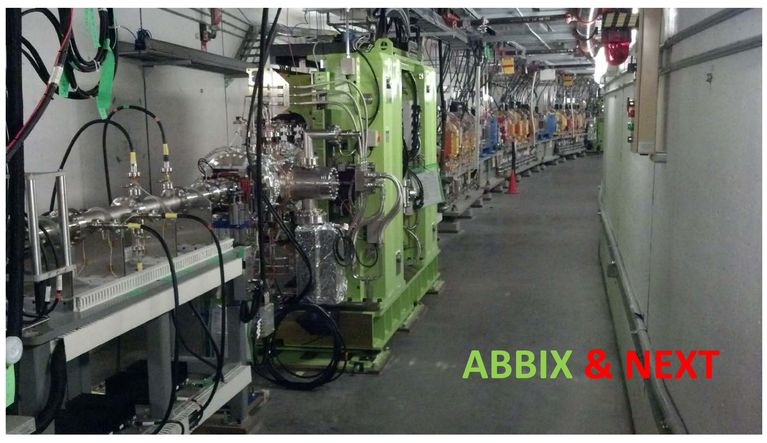

1.4-m Two-array EPU57 and 2.7-m Quasi-periodic EPU105 for ESM

3.5-m Two-array EPU57 for SIX

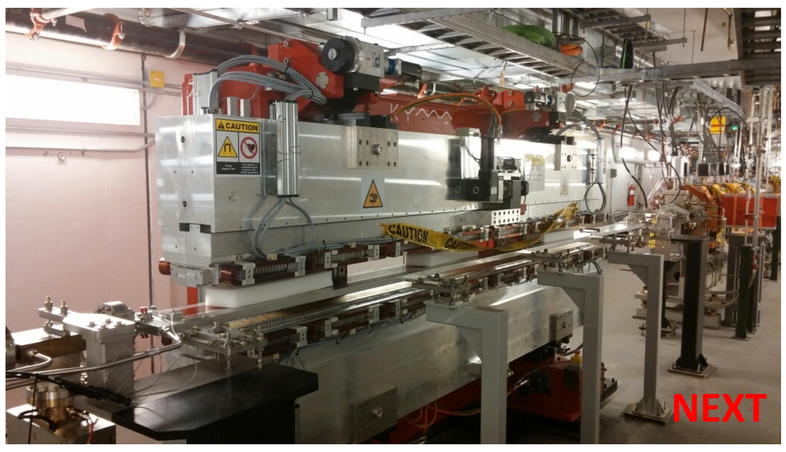

3PW (BDN & Partner)

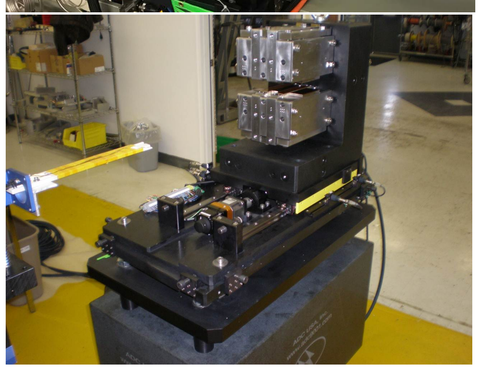

Refurbished IVU18 from NSLS (NYX)

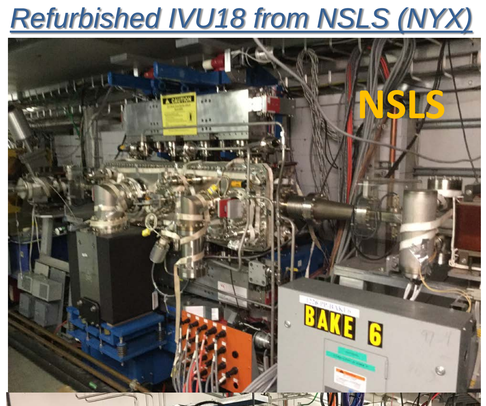

Refurbished U42 from ESRF (SST)

EPU60 from SRC to be rebushied (SST)

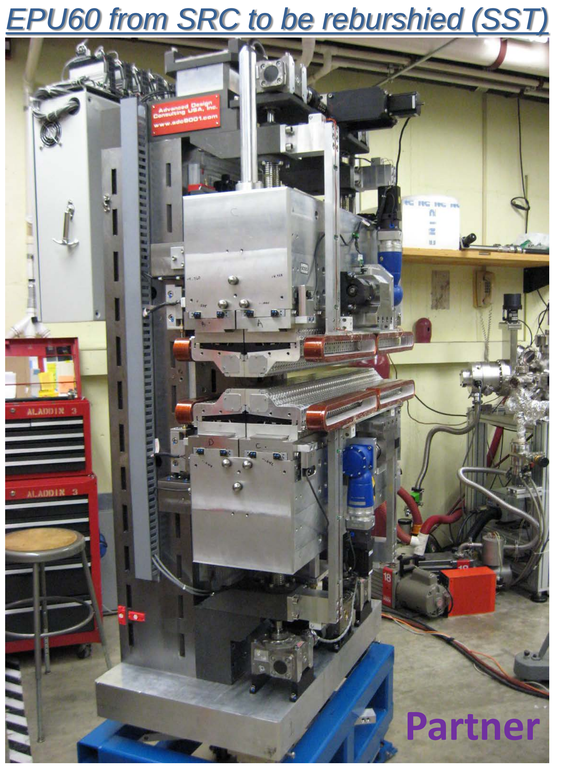

Lossless Crossing of a Resonance Stopband during Tune Modulation by Synchrotron Oscillations

G.M. Wang#, T. Shaftan, Y. Li , V. Smaluk

Brookhaven National Laboratory, Upton, NY, 11973 USA

Abstract

Modern high performance circular accelerators require sophisticated nonlinear corrections. The beam betatron tune footprint may cross many resonances, which may cause particle loss and reduce dynamic aperture. However, if a beam crosses a resonance reasonably fast, the beam deterioration may be minimized. This paper describes the experiments with the beam passing through a half-integer resonance stopband via tune modulation by exciting synchrotron oscillations. This is the first time that beam dynamics was under precise control while the beam crossed the half-integer resonance. Our results convincingly demonstrate that particles can cross a half-integer resonance without being lost if the passage is reasonable fast and the resonance stopband is sufficiently narrow.

Introduction

. The common practice of the lattice design is to place the machine tunes clear of major resonances on tune diagram [1].

. Tune confinement approach: fit tune footprint due to on-energy and off-energy tune spread between the resonance stopbands so that it does not overlap with them or cross them.

. The half-integer resonance poses concerns in many circular accelerators, such as modern synchrotron light sources, heavy ion medical accelerators and non-scaling fixed-field alternating-gradient (FFAG) accelerators

.MBA lattice (such as APS-U, HEPS): off-energy tunes for the chosen lattices spread across the major resonances including the half-integer stopband.

. Surprisingly this does not cause the particle loss in tracking. For the APS-U lattice having large chromatic range of betatron tunes helps in securing large momentum aperture, which, in turn, leads to a long beam lifetime.

.The authors of [2] concluded that the reason behind the lossless crossing of ½ resonance is the rapid transition from one side of the stopband to another together with substantial tune shifts with amplitude that help to drive particle off the resonance during the transition. Results of our studies indicate that this explanation is adequate.

.Significance of the finding from simulation advances the modern lattice design beyond the principles of the "tune confinement", while posing an important question: under which conditions does the chromatic tune footprint not need to be confined?

.We investigate, both theoretically and experimentally, the beam dynamics during crossing of a major resonance in one of the lowest-emittance storage rings worldwide. This is the first time in experiments carried out in the storage rings that beam was crossing the half-integer resonance without losses due to fast passage and narrow resonance stopband width.

Dynamics of the particle crossing a resonance stopband

. Storage ring with large chromatic tune shift

$$\nu(\delta) = \nu_0 + \xi_1\delta + \xi_2\delta^2 + O(\delta^3)$$

. 2-D case (y, δ)

. Consider lattice with small tune-amplitude dependence.

. Particle kicked with synchrotron oscillation

$$\delta(t) = \delta_0 \sin(2\pi\nu_s n)$$

. A cartoon to show the beam betatron tune crosses the resonance during longitudinally oscillation.

. Resonance is not infinitely thin in presence of quadrupole errors. The resonance is characterized by a stopband width Δn_R.

. The number of turns the particle will take to cross the stopband depends on stopband width, chromaticity and energy oscillation amplitude.

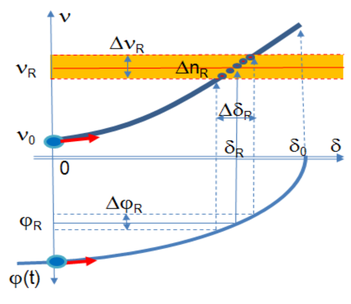

Particle crossing resonance with synchrotron oscillations

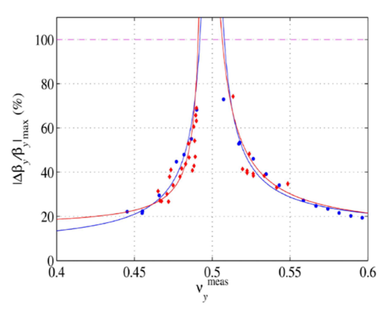

Measurement of stopband width at NSLS-II

Controlling the resonance stopband width

. Stopband width is defined by quadrupole errors

. Quadrupole errors changed tune (0^{th} harmonic) and defined finite stopband width (p^{th} harmonic)

$$\Delta\nu_t = \frac{1}{4\pi}\sum_q \beta_q(\Delta k_1 L)_q \qquad J_p = \frac{1}{2\pi}\left|\sum_q \beta_q(\Delta k_1 L)_q e^{-ip\phi_q}\right|$$

. The resonance stopband width is heuristically defined as the boundary of the tune range where the peak beta-beat reaches 100%

. Increase stopband width by controlling harmonic quadrupoles strength

. Characterized stopband width by measuring beta-beat

. Position tune close 1/2 resonance

. Changed ring quads K1 to move tune crossing 1/2

. Changed RF frequency to move tune crossing 1/2

. NSLS-II stopband width is 0.016 with natural lattice beta beat at ~3%

Parametric oscillator excited at ½ resonance

. Hill's equation with normalized variables

$$\frac{d^2\eta}{d\phi^2} + (\nu + \delta\nu)^2\eta = -\nu^2\beta^2\Delta k_1(\phi)\eta$$

. Solution

. Outside stopband

$$\eta(\tau) = \sqrt{2(C_1^2 + C_2^2)}\left[\mu_1 \sin(\lambda\tau + \varphi_0)\cos\frac{\tau}{2} + \lambda\cos(\lambda\tau + \varphi_0)\sin\frac{\tau}{2}\right]$$

. Within stopband

$$\eta(\tau) = C_1\sqrt{\mu_1^2 + \lambda^2}e^{\lambda\tau}\sin\left(\frac{\tau}{2} + \varphi_0\right) - C_2\sqrt{\mu_1^2 + \lambda^2}e^{-\lambda\tau}\sin\left(\frac{\tau}{2} - \varphi_0\right)$$

. Tune position relative to the stopband width defines the types of beam motion: exponential growth or stable periodic oscillation

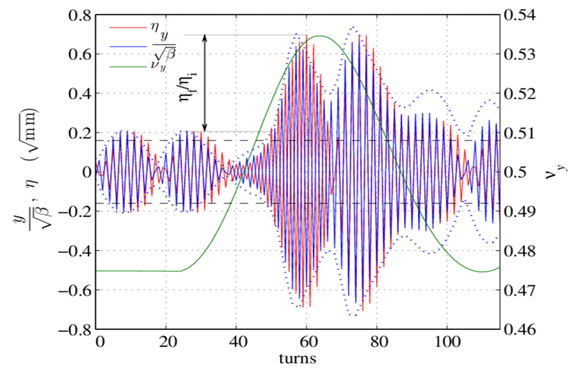

Betatron oscillation amplitude versus turn number: numerical solution (red curve) and particle tracking with Elegant (blue curve)

Experiment result

. Set the lattice with large ξ_2 =300

. Position y plane tune close to 1/2 resonance

. Aligned SR BPMs TBT data with transverse pinger and RF pinger

. Transverse pinger excited betatron parametric oscillation for independent measurement of the detune together with well-controlled initial conditions.

. RF pinger excited beam synchrotron oscillation

. Beam acts as one giant particle

. Dispersion BPM TBT beam X/Y/I position measured the beam TBT energy oscillation, amplitude growth during half integer cross and beam loss.

. Controlled the stopband width: small (0.016) and large (0.038)

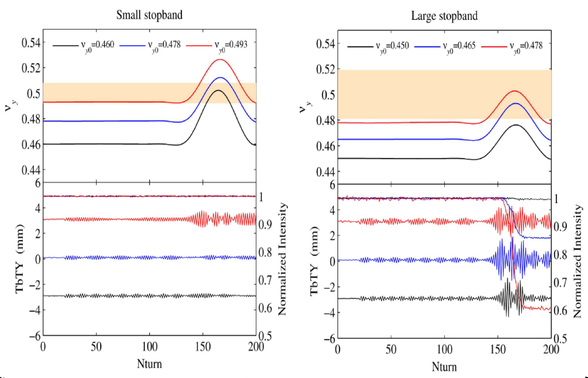

Turn-by-turn beam parameters (upper plot: calculated y-tunes with the stopband represented by the shaded area, lower plot: BPM measured TBT y-position measured on left axis and normalized beam intensity on right axis) for the three separate experiments with three different initial tunes

Conclusion

. It may be unnecessary to confine the chromatic tune footprint between the resonance stopbands. The storage rings with a large chromatic tune swing can yet successfully reach large momentum aperture provided that two conditions are satisfied.

. The first condition states that the resonance stopbands need to be corrected well by manufacturing and aligning of magnets with small residual field errors and accurate cancellation of the harmful error harmonics.

. The other condition is in maintaining large magnitude of high order chromaticity.

. Combination of the two conditions above lead to a rapid crossing of the resonance stopband, which does not cause loss of the particles as demonstrated by our experiments.

Acknowledgment

We are grateful to F. Willeke and S.Y. Lee for helpful discussions and advice. We appreciate the NSLS-II RF group help for RF pinger.

gwang@bnl.gov DOE contract No: DE-AC02-98CH10886

AC LOCO

X. Yang, V. Smaluk, L.H. Yu, Y. Tian, K. Ha

Abstract

A novel technique has been developed to improve the precision and shorten the measurement time of the LOCO (Linear Optics from Closed Orbits) method. This technique, named AC LOCO, is based on sine-wave (AC) beam excitation via fast correctors. Such fast correctors are typically installed at synchrotron light sources for the fast orbit feedback. The beam oscillations are measured by beam position monitors. The narrow band used for the beam excitation and measurement not only allows us to suppress effectively the beam position noise, but also opens the opportunity for simultaneously exciting multiple correctors at different frequencies (multi-frequency mode). We demonstrated at NSLS-II that AC LOCO provides better lattice corrections and works much faster than the traditional LOCO method.

Measurement Technique

A standard synchronous detection technique for the BPM data processing

$$U_{\mathrm{ref}}(t) = a_{\mathrm{ref}} \sin(\omega_0 t + \varphi_{\mathrm{ref}})$$
$$U_{\mathrm{bpm}}(t) = a_{\mathrm{bpm}} \sin(\omega_0 t + \varphi_{\mathrm{bpm}}) + \varepsilon(t).$$

$$U_{\mathrm{mix}} = U_{\mathrm{ref}} U_{\mathrm{bpm}}$$
$$\overline{U_{\mathrm{mix}}} \equiv \frac{1}{T}\int_0^T U_{\mathrm{mix}}(t)\,dt$$

$$a_{\mathrm{bpm}} = \frac{2\overline{U_{\mathrm{mix}}}}{a_{\mathrm{ref}} \cos(\varphi_{\mathrm{bpm}} - \varphi_{\mathrm{ref}})} - \delta a$$
$$\delta a = \frac{2\int_0^T \varepsilon(t) \sin(\omega_0 t + \varphi_{\mathrm{ref}})\,dt}{T \cos(\varphi_{\mathrm{bpm}} - \varphi_{\mathrm{ref}})}$$

Accuracy Analysis

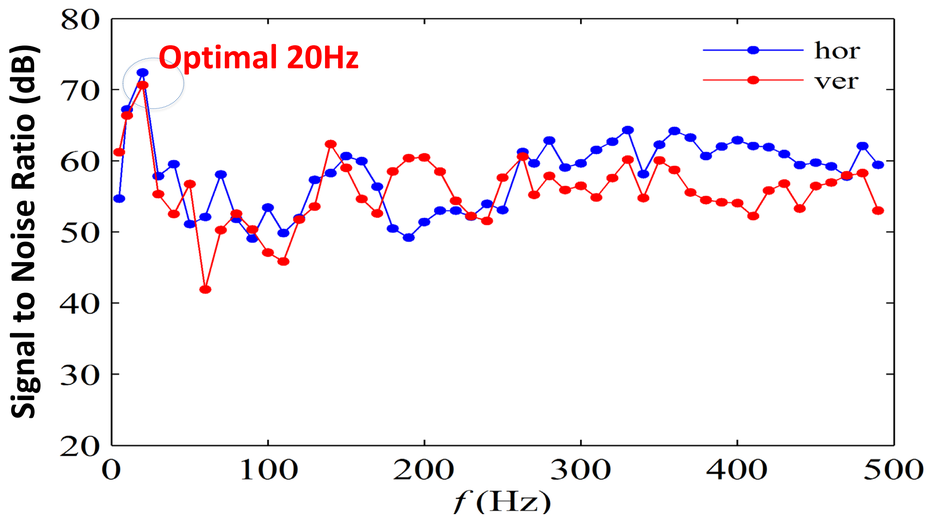

Figure 1: Measured single-to-noise ratio vs frequency: horizontal (blue) and vertical (red).

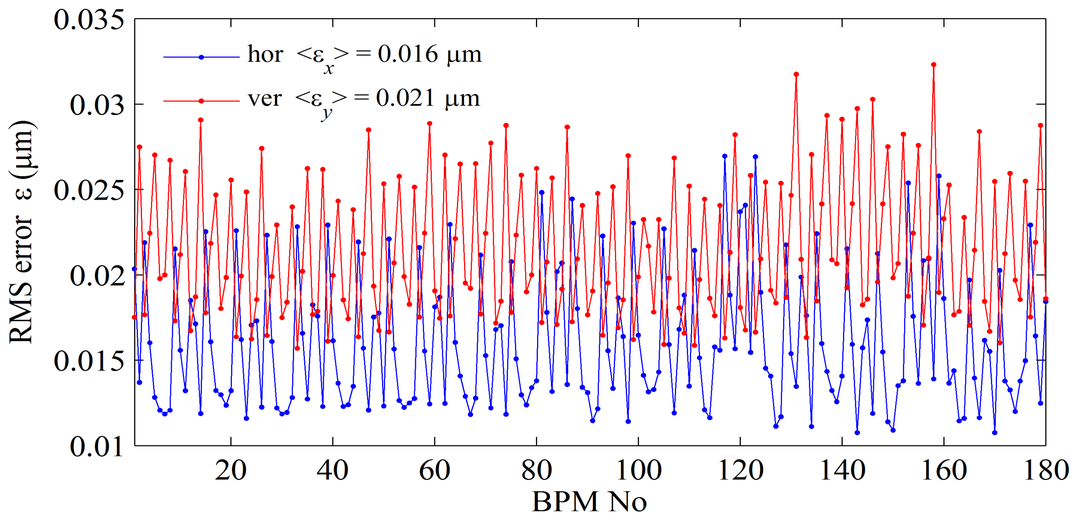

Figure 2: RMS amplitude errors at 20 Hz.

Multi-frequency Excitation

Since the signal bandwidth is quite small (0.2 Hz for a 5 second measurement), it provides a unique opportunity to simultaneously excite the beam oscillation via multiple correctors with different frequencies separated by an interval of Δf. Proof-of-principle experiment has been carried out at NSLSII. It takes < 2 min for a complete set of LOCO measurement, which is comparable to the TbT based methods, also with at least an order of magnitude improved measurement precision.

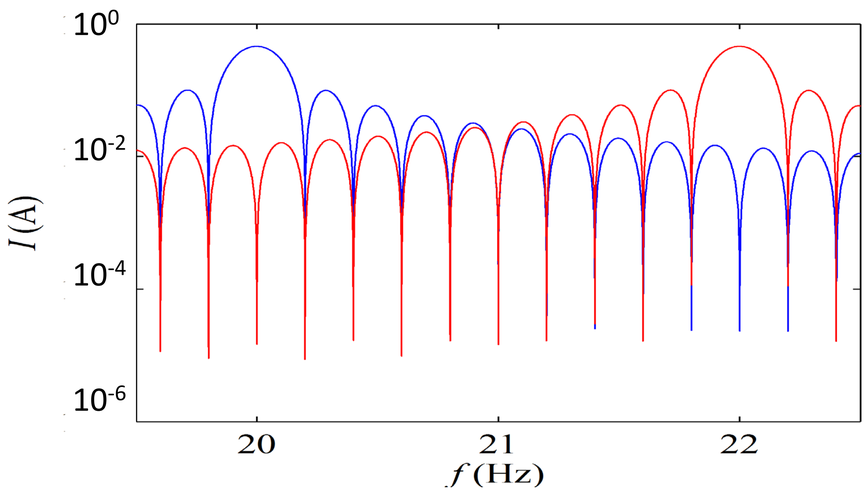

Figure 3: Spectra of fast corrector excitation signals.

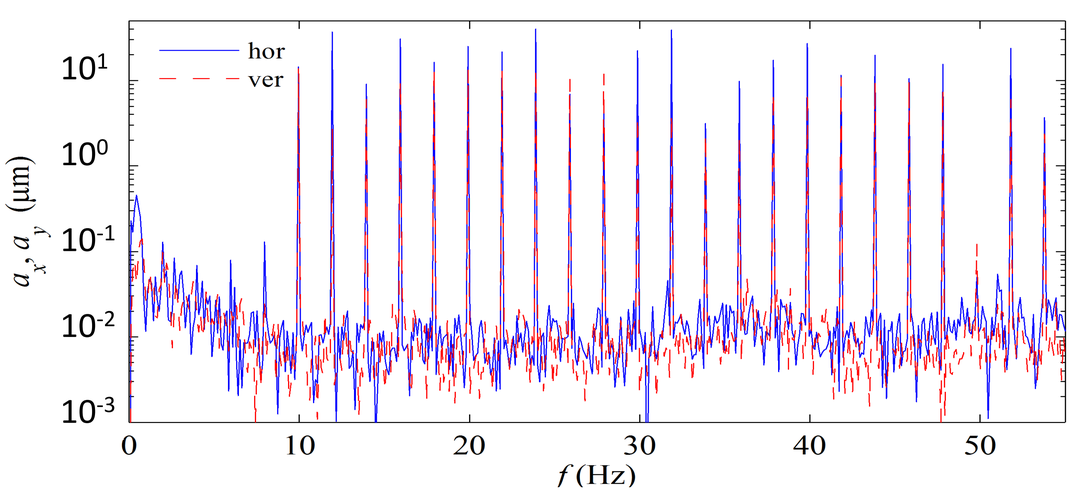

Figure 4: Amplitude spectra of horizontal (blue) and vertical (red) BPM signals.

Experimental Results

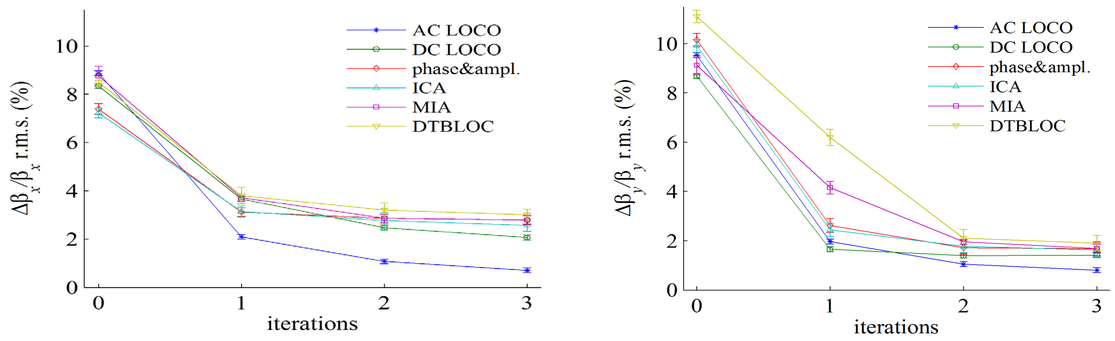

Figure 5: Convergence of beta function: horizontal (left) and vertical (right).

Conclusion

A fast and precise AC LOCO technique of magnet lattice correction has been developed. AC LOCO achieves a measurement precision of 15 nm and it takes only few minutes compared to the conventional LOCO with a precision of 1 μm and a measurement time of 1 hour. The significantly improved accuracy of the ORM measurement results in a reduction in the residual beta function errors of the corrected linear lattice by a factor of two. Further reduction of the measurement time is achieved by driving multiple correctors with different frequencies simultaneously. At NSLS-II, we have carried out a proof-of-principal experiment of the multi-frequency excitation of 30 correctors. We were able to keep the measurement accuracy in the nanometer level for all the excitation frequencies in the 10 – 68 Hz range. Based on the LOCO simulation results, the achieved high precision could open the door for finding sextupole alignment errors.

Analysis of Nonlinear Dynamics by Square Matrix Method

Li Hua Yu, Yongjun Li
Brookhaven National Laboratory

NATIONAL SYNCHROTRON LIGHT SOURCE II

Write one turn map of Taylor expansion as square matrix

L. H. Yu, PRAB. 20, 034001 (2017)

Simplest example of nonlinear map :

$$x = x_0\cos\mu + p_0\sin\mu + \epsilon x_0^2\sin\mu$$
$$p = -x_0\sin\mu + p_0\cos\mu + \epsilon x_0^2\cos\mu$$

Use $z = x - ip$ and $z^* = x + ip$

$$z = e^{i\mu}z_0 - \frac{i}{4}\epsilon e^{i\mu}z_0^2 - \frac{i}{2}\epsilon e^{i\mu}z_0z_0^* - \frac{i}{4}\epsilon e^{i\mu}z_0^{*2}$$
$$z^* = e^{-i\mu}z_0^* + \frac{i}{4}\epsilon e^{-i\mu}z_0^2 + \frac{i}{2}\epsilon e^{-i\mu}z_0z_0^* + \frac{i}{4}\epsilon e^{-i\mu}z_0^{*2}$$
$$z^2 = e^{2i\mu}z_0^2 - \frac{i}{2}\epsilon e^{2i\mu}z_0^3 - i\epsilon e^{2i\mu}z_0^2z_0^* - \frac{i}{2}\epsilon e^{2i\mu}z_0z_0^{*2}$$
$$zz^* = z_0z_0^* + \frac{i}{4}\epsilon z_0^3 + \frac{i}{4}\epsilon z_0^2z_0^* - \frac{i}{4}\epsilon z_0z_0^{*2} - \frac{i}{4}\epsilon z_0^{*3}$$
$$z^{*2} = e^{-2i\mu}z_0^{*2} + \frac{i\epsilon}{2}e^{-2i\mu}z_0^2z_0^* + i\epsilon e^{-2i\mu}z_0z_0^{*2} + \frac{i\epsilon}{2}e^{-2i\mu}z_0^{*3}$$
$$z^3 = e^{3i\mu}z_0^3$$
$$\ldots$$
$$z^{*3} = e^{-3i\mu}z_0^{*3}$$

$$\tilde{Z} = (1, z, z^*, z^2, zz^*, z^{*2}, z^3, z^2z^*, zz^{*2}, z^{*3}). \longrightarrow Z = MZ_0,$$

At 3rd order M is 10x10 matrix:

$$M = \begin{bmatrix} 1 & 0 & 0 & 0 \\ 0 & M_{11} & M_{12} & M_{13} \\ 0 & 0 & M_{22} & M_{23} \\ 0 & 0 & 0 & M_{33} \end{bmatrix}$$

$$M_{11} = \begin{bmatrix} e^{i\mu} & 0 \\ 0 & e^{-i\mu} \end{bmatrix}, M_{22} = \begin{bmatrix} e^{2i\mu} & 0 & 0 \\ 0 & 1 & 0 \\ 0 & 0 & e^{-2i\mu} \end{bmatrix}, \ldots$$

$$M_{23} = \begin{bmatrix} -\frac{i}{2}\epsilon e^{2i\mu} & -i\epsilon e^{2i\mu} & -\frac{i}{2}\epsilon e^{2i\mu} & 0 \\ \frac{i}{4}\epsilon & \frac{i}{4}\epsilon & -\frac{i}{4}\epsilon & -\frac{i}{4}\epsilon \\ 0 & \frac{i}{2}\epsilon e^{-2i\mu} & i\epsilon e^{-2i\mu} & \frac{i}{2}\epsilon e^{-2i\mu} \end{bmatrix}$$

M is upper-triangular matrix with diagonal elements precisely known (the eigenvalues)

$1, \{e^{i\mu}, e^{-i\mu}\}, \{e^{2i\mu}, 1, e^{-2i\mu}\}, \{e^{3i\mu}, e^{i\mu}, e^{-i\mu}, e^{-3i\mu}\}$ -->2 eigenvectors

- Invariant subspace of eigenvalue $e^{i\mu}$ of dimension 2.
- In 3rd order, nonlinear dynamics is represented by a rotation in this 2 dimensional space
  10x10→2x2
- For higher order, the dimension of the invariant subspace is always much smaller than original dimension.
- Example, 7'th order , for 4 variables x, p_x, y, p_y
  330x330→4x4

We find left eigenvectors U, such that with Jordan matrix τ

$$UM = e^{i\mu I + \tau}U \qquad U = \begin{bmatrix} u_1 \\ u_2 \\ \ldots \\ \ldots \\ u_{m-1} \end{bmatrix} \qquad \tau = \begin{bmatrix} 0 & 1 & 0 & \ldots & 0 \\ 0 & 0 & 1 & \ldots & 0 \\ 0 & \ldots & \ldots & \ldots & 0 \\ 0 & 0 & 0 & \ldots & 1 \\ 0 & 0 & 0 & \ldots & 0 \end{bmatrix}$$

There is **only one step to high order**, without iteration from low order to high order

- Example, 3'th order , for 2 variables
  U: 2x10 matrix M: 10x 10 τ: 2x2 matrix
- Example, 7'th order , for 4 variables
  U: 4x330 matrix M: 330x 330 τ : 4x4 matrix

$$UZ = UMZ_0 = e^{i\mu I + \tau}UZ_0. \qquad \text{Let} \quad W \equiv UZ = \begin{bmatrix} w_0 \\ w_1 \\ \ldots \\ w_{m-1} \end{bmatrix}$$

$$W \equiv UZ,\ W_0 \equiv UZ_0 \longrightarrow W = e^{i\mu I + \tau}W_0.$$

KAM theory states that the invariant tori are stable under small perturbation
There is a stable frequency, hence

$W = e^{i\mu I + \tau}W_0 \cong e^{i(\mu+\phi)}W_0.$ (I here is the identity matrix)

Compare left with right side

$\tau W_0 \cong i\phi W_0.$

So we must have an approximate "Coherent state":

$$\tau \begin{bmatrix} w_0 \\ w_1 \\ \ldots \\ w_{m-1} \end{bmatrix} = \begin{bmatrix} w_1 \\ w_2 \\ \ldots \\ 0 \end{bmatrix} \cong \begin{bmatrix} i\phi w_0 \\ i\phi w_1 \\ \ldots \\ i\phi w_{m-1} \end{bmatrix} \longrightarrow i\phi = \frac{w_1}{w_0} \cong \frac{w_2}{w_1} \cong \frac{w_3}{w_2} \cdots \frac{w_{m-1}}{w_{m-2}}$$

(Last row is very small, so it is still approximately correct)

Amplitude dependent tune ϕ

Action $|w_0|$ **is nearly a constant**

The Pendulum Equation as an 3rd order example

$H = \frac{p^2}{2} + 1 - \cos(x)$ $\quad H = \frac{p^2}{2} + \frac{x^2}{2} - \frac{x^4}{24}$ Expand Hamiltonian to 4'th order

$z \equiv x - ip, \quad z^* \equiv z + ip$

$$\dot{z} = iz - \frac{iz^3}{48} - \frac{1}{16}iz^2z^* - \frac{1}{16}izz^{*2} - \frac{iz^{*3}}{48}$$
$$\dot{z^*} = -iz^* + \frac{iz^{*3}}{48} + \frac{1}{16}iz^*z^{*2} + \frac{1}{16}iz^2z^* + \frac{iz^3}{48}$$
$$\frac{dz^2}{dt} \approx 2iz^2, \quad \frac{dzz^*}{dt} \approx 0, \quad \frac{dz^{*2}}{dt} \approx 2iz^{*2}, \quad \cdots, \quad \frac{dz^{*3}}{dt} \approx -3iz^{*3}$$

$$M = \begin{pmatrix} 0&0&0&0&0&0&0&0&0&0 \\ 0&i&0&0&0&0&-\frac{i}{48}&-\frac{i}{16}&-\frac{i}{16}&-\frac{i}{48} \\ 0&0&-i&0&0&0&\frac{i}{48}&\frac{i}{16}&\frac{i}{16}&\frac{i}{48} \\ 0&0&0&2i&0&0&0&0&0&0 \\ 0&0&0&0&0&0&0&0&0&0 \\ 0&0&0&0&0&-2i&0&0&0&0 \\ 0&0&0&0&0&0&3i&0&0&0 \\ 0&0&0&0&0&0&0&i&0&0 \\ 0&0&0&0&0&0&0&0&-i&0 \\ 0&0&0&0&0&0&0&0&0&-3i \end{pmatrix}$$

$$U = \begin{pmatrix} u_0 \\ u_1 \end{pmatrix} = \begin{pmatrix} 0&1&0&0&0&0&\frac{1}{96}&0&-\frac{1}{32}&-\frac{1}{192} \\ 0&0&0&0&0&0&0&-\frac{i}{16}&0&0 \end{pmatrix}$$ Left eigenvectors

$$\dot{Z} = MZ, \quad UM = (i\omega_0 I + \tau)U, \quad \tau \equiv \begin{bmatrix} 0 & 1 \\ 0 & 0 \end{bmatrix}.$$

$$W = UZ = \begin{bmatrix} u_0Z \\ u_1Z \end{bmatrix} \equiv \begin{bmatrix} w_0 \\ w_1 \end{bmatrix}.$$

$$\dot{W} = U\dot{Z} = UMZ = (i\omega_0 I + \tau)UZ = (i\omega_0 I + \tau)W$$

$$\dot{w_0} = i\omega_0 w_0 + w_1 = (i\omega_0 + \frac{w_1}{w_0})w_0 \equiv i(\omega_0 + \phi)w_0$$
$$\dot{w_1} = i\omega_0 w_1$$

$$w_0 = u_0Z = z + \frac{z^3}{96} - \frac{zz^{*2}}{32} - \frac{z^{*3}}{192} \approx z$$
$$w_1 = u_1Z = -\frac{1}{16}iz^2z^*$$

Lowest order approximation

$$\Delta\omega = \phi = -i\frac{w_1}{w_0} \cong -\frac{1}{16}zz^*$$ Frequency shift

$$E_0 = \frac{z^2}{2}, \quad \omega_0 = 1 \quad \text{, and initially,} \quad z^* = z = x_0 \quad \text{, so}$$

$$\frac{\omega}{\omega_0} = \frac{\omega_0 + \Delta\omega}{\omega_0} \cong 1 - \frac{1}{8}E_0$$ A well known result

This is at 3'rd order. At 9'th order,

$$\frac{\omega}{\omega_0} = 1 - \frac{E_0}{8} - \frac{5E_0^2}{256} - \frac{11E_0^3}{2048} - \frac{21233E_0^4}{11796480}$$

Chirikov use super-convergent canonical perturbation theory
To get this

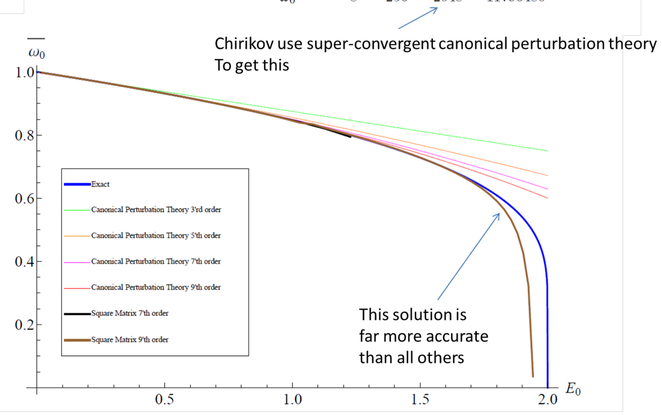

Compare canonical perturbation theory with Square Matrix

Multi-turns

$W(n) = e^{in\mu}e^{n\tau}W_0$

Further derivation leads to

$w_0(n) = e^{in\mu + in\phi + \frac{n^2}{2}\Delta + \cdots}w_0(n=0)$

$\Delta \equiv \frac{w_2}{w_0} - (\frac{w_1}{w_0})^2$ ≈0

Gives **frequency fluctuation**, seems to be related to Liapunov exponent.

"Coherence condition":

$\mathrm{Im}\phi \approx 0; \Delta \approx 0.$

Numerical Test, Poincare Sections: Strongly coupled x,y motion reduced to two simple independent rotations in separate planes

$z_x = J_x e^{i\psi_x}, z_y = J_y e^{i\psi_y}$ Courant-Snyder actions vary

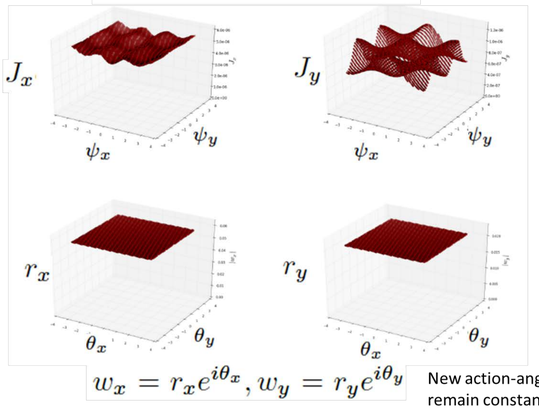

Initial x=10mm, y=2mm

$w_x = r_x e^{i\theta_x}, w_y = r_y e^{i\theta_y}$ New action-angle variables remain constant

Tune vz. Amplitude agrees with tracking

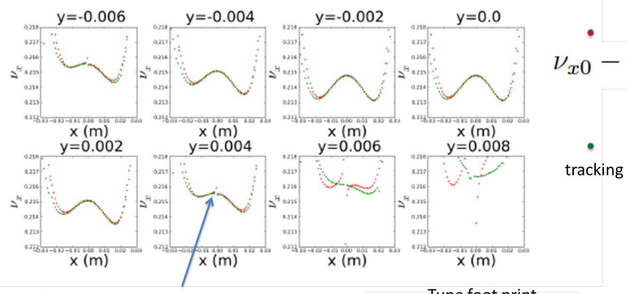

"Coherence condition"

$\Delta \equiv \frac{w_2}{w_0} - (\frac{w_1}{w_0})^2$ ≈0

Gives frequency fluctuation, seems to be related to Liapunov exponent.

Δ_x Compared with ⟶ Frequency map, obtained by heavy tracking Calculation (Yongjun Li)

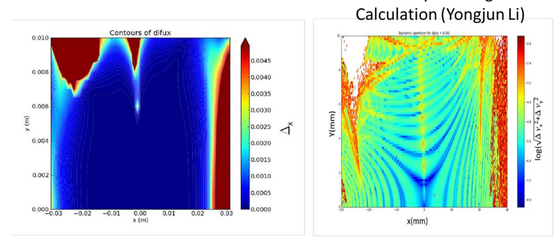

This can be used to optimize "dynamic aperture" of storage rings

Phase space manipulation

5 particles with initial y increases proportional to initial x
Before and after minimization of $|\Delta w/w|$ by Yongjun Li

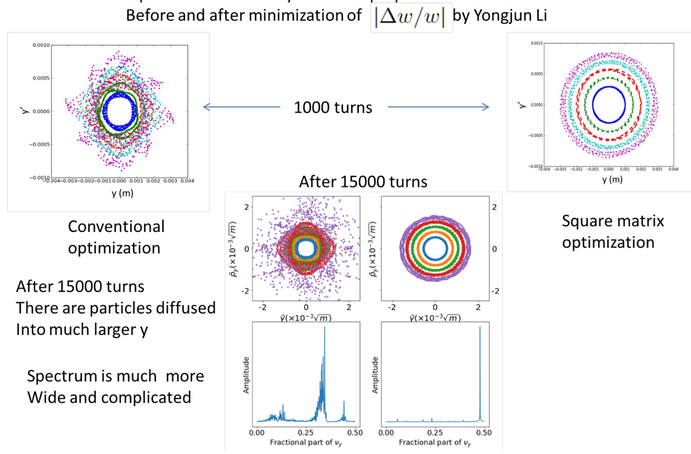

Conventional optimization

After 15000 turns
There are particles diffused
Into much larger y

Spectrum is much more
Wide and complicated

Square matrix optimization

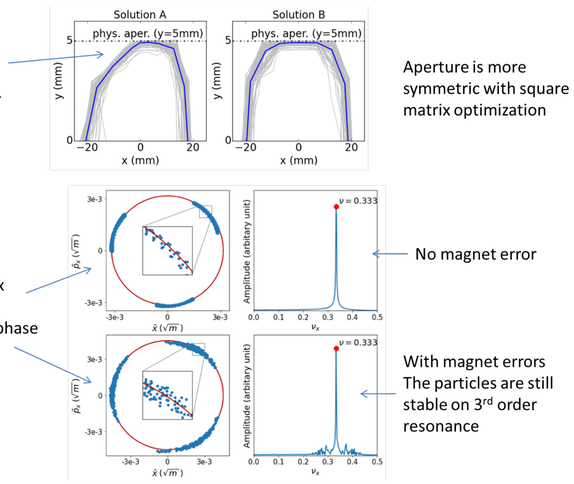

Tune footprint comparison of two approaches

Optimized by nonlinear driving terms

Optimization obtained by square matrix

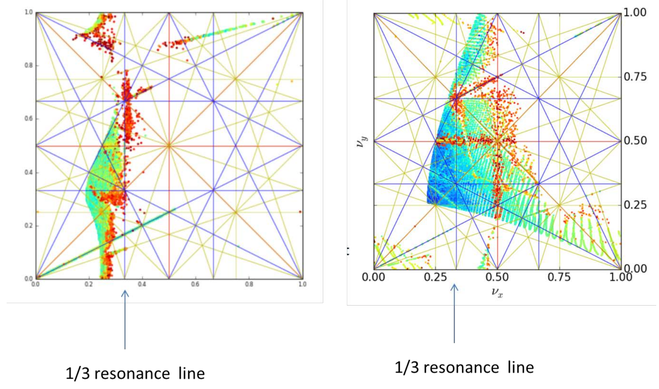

Summary of off Resonance solution

- Square matrix $Z = MZ_0$
- One step to high order without iteration $UM = e^{i\mu I + \tau}U$
- Action-angle approximation $W \equiv UZ = \begin{bmatrix} w_0 \\ w_1 \\ \ldots \\ w_{m-1} \end{bmatrix}$
  $W = e^{i\mu I + \tau}W_0 \cong e^{i(\mu+\phi)}W_0.$
- **Amplitude dependent tune** φ
  Action $|w_0|$ **is nearly a constant:** $|\frac{\Delta W}{W}| \approx 0$
- **frequency fluctuation** $\Delta \equiv \frac{w_2}{w_0} - (\frac{w_1}{w_0})^2$ ≈0
  amplitude fluctuation $|\frac{\Delta W}{W}|$
- "Coherence condition": $\mathrm{Im}\phi \approx 0; \Delta \approx 0.$ $|\frac{\Delta W}{W}| \approx 0$